Pacific Northwest
NATIONAL LABORATORY

SERDP WP18-1660 Final Report

Revealing Bilgewater Emulsion Formation and Breaking by In Situ Multiplexed Chemical Imaging and Microfluidics

June 2020

Xiao-Ying Yu

U.S. DEPARTMENT OF ENERGY

Prepared for the U.S. Department of Energy
under Contract DE-AC05-76RL01830

REPORT DOCUMENTATION PAGE

Form Approved
OMB No. 0704-0188

1. REPORT DATE *(DD-MM-YYYY)*	2. REPORT TYPE	3. DATES COVERED *(From - To)*
07/31/2019	SERDP Final Report	

4. TITLE AND SUBTITLE
Revealing Bilgewater Emulsion Formation and Breaking by In Situ Multiplexed Chemical Imaging and Microfluidics

5a. CONTRACT NUMBER
DE-AC05-76RL01830

5b. GRANT NUMBER

5c. PROGRAM ELEMENT NUMBER

6. AUTHOR(S)
Xiao-Ying Yu

5d. PROJECT NUMBER
WP18-1660

5e. TASK NUMBER

5f. WORK UNIT NUMBER

7. PERFORMING ORGANIZATION NAME(S) AND ADDRESS(ES)
Pacific Northwest National Laboratory
902 Battelle Blvd.
Richland, WA 99352

8. PERFORMING ORGANIZATION REPORT NUMBER
WP18-1660

9. SPONSORING/MONITORING AGENCY NAME(S) AND ADDRESS(ES)
Strategic Environmental Research and Development Program
4800 Mark Center Drive, Suite 17D03
Alexandria, VA 22350-3605

10. SPONSOR/MONITOR'S ACRONYM(S)
SERDP

11. SPONSOR/MONITOR'S REPORT NUMBER(S)
WP18-1660

12. DISTRIBUTION/AVAILABILITY STATEMENT
DISTRIBUTION STATEMENT A. Approved for public release: distribution unlimited.

13. SUPPLEMENTARY NOTES

14. ABSTRACT Bilgewater, an oil and grease mixture with water, may affect many aquatic species. Thus development of methods and techniques to treat (i.e., increase OWS availability, reduce cost) or to mitigate the formation and undesired consequences of shipboard emulsions are urgently needed. This research aims to investigate the fundamental physicochemical processes in the formation, stabilization, and breaking of shipboard relevant emulsions. Understanding shipboard emulsions at evolving interfaces is a key scientific challenge. The underpinning hypothesis is that surface chemical changes at the l-l interface are critical for mass and charge transfer leading to emulsion formation, stabilization, and worsening. Using unique in situ chemical imaging capabilities developed at PNNL, the project team answers the following questions to validate the following questions: 1) How do ionic, nonionic, and solid emulsifiers affect emulsion stabilization in ship bilgewater conditions? and 2) How does microbial activity affect emulsion formation, stabilization, and breaking? A unique vacuum compatible microreactor, System for Analysis at the Liquid Vacuum Interface (SALVI), has been used to achieve multiscale imaging and obtain a more fundamental understanding of these physiochemical multiphase processes.

15. SUBJECT TERMS
Bilgewater Emulsion Formation, In Situ Multiplexed Chemical Imaging, Microfluidics

16. SECURITY CLASSIFICATION OF:			17. LIMITATION OF ABSTRACT	18. NUMBER OF PAGES	19a. NAME OF RESPONSIBLE PERSON
a. REPORT	b. ABSTRACT	c. THIS PAGE			Xiao-Ying Yu
					19b. TELEPHONE NUMBER *(Include area code)*
UNCLASS	UNCLASS	UNCLASS	UNCLASS	47	509-372-4524

Tabe of Content

1.0 Acknowledgement

This research is supported by the SERDP project WP18-1660. The project team consists of Dr. Jiyoung Son, Dr. George Bonheyo, Dr. Kee Sung Han, Ms. Jenn Yao, Ms. Yanjie Shen, and Ms. Rachel Komorek, all of Pacific Northwest National Laboratory. We also thank our Navy collaborator Danielle Paynter and her group for providing the emulsion recipe and key ingredients. We are grateful for support and assistance from Ginny Collier and Janie Vickerman in monthly spending reports. We thank Mark Freshley and Jill Brandenberger for programmatic support. We used the EMSL general user proposal 51176 to have access to advanced imaging platforms for this work.

2.0 SERDP Relevance

This research will provide fundamental understanding of the underlying principles of bilgewater emulsion formation, stabilization, and breaking using multiplexed in situ chemical imaging techniques to study, at the molecular level, the l-l interactions and liquid surface modifications under ship-relevant conditions. Findings, based on direct observations, will provide physical and chemical knowledge underpinning these complex interfacial phenomena and lead to solutions for oil in water (O/W) emulsion reduction, improved wastewater treatment, waste-oil-holding capacities, and fuel-holding capacities onboard ships. Microfluidic-based strategies for stabilization, effective separation, and treatment of O/W emulsions, which will be developed based on the findings of this research, can reduce maintenance burden, increase OWS treatment efficiency, and lower the cost of wastewater treatment for DOD.

This research will provide fundamental understanding of the underlying principles of bilgewater emulsion formation, stabilization, and breaking using multiplexed in situ chemical imaging techniques to study, at the molecular level, the l-l interactions and liquid surface modifications under ship-relevant conditions. Findings, based on direct observations, will provide physical and chemical knowledge underpinning these complex interfacial phenomena and lead to solutions for oil in water (O/W) emulsion reduction, improved wastewater treatment, waste-oil-holding capacities, and fuel-holding capacities onboard ships. Microfluidic-based strategies for stabilization, effective separation, and treatment of O/W emulsions, which will be developed based on the findings of this research, can reduce maintenance burden, increase OWS treatment efficiency, and lower the cost of wastewater treatment for DOD.

3.0 Technical Objective

Bilgewater, an oil and grease mixture with water, may affect many aquatic species. Thus development of methods and techniques to treat (i.e., increase OWS availability, reduce cost) or to mitigate the formation and undesired consequences of shipboard emulsions are urgently needed. This research aims to investigate the fundamental physicochemical processes in the formation, stabilization, and breaking of shipboard relevant emulsions. Understanding shipboard emulsions at evolving interfaces is a key scientific challenge. The underpinning hypothesis is that surface chemical changes at the l-l interface are critical for mass and charge transfer leading to emulsion formation, stabilization, and worsening. Using unique in situ chemical imaging capabilities developed at PNNL, we answer the following questions to validate the following questions: 1) How do ionic, nonionic, and solid emulsifiers affect emulsion stabilization in ship bilgewater conditions? and 2) How does microbial activity affect emulsion formation, stabilization, and breaking? A unique vacuum compatible microreactor, System for Analysis at the Liquid Vacuum Interface (SALVI),[1-8] has been used to achieve multiscale imaging and obtain a more fundamental understanding of these physiochemical multiphase processes.

This project aims to achieve the following goals: 1) study the emulsion formation mechanism in synthetic and actual bilgewater using novel multimodal imaging approaches; 2) obtain molecular distribution of key species at the droplet surface and interface; and 3) set the technical foundation for the development of cost-effective solutions to reduce, prevent, and treat ship-relevant emulsions.

4.0 Technical Approach

The key technical approach is to use SALVI, a unique vacuum and ambient compatible microfluidic interface [1-8] and multimodal imaging to study emulsion. We have employed in situ liquid chemical imaging to study various liquid surfaces, solid-liquid (s-l), and l-l interfaces [3, 5, 6, 8-15]. SALVI, as a portable microfluidic reactor, is suitable for a multitude of analytical instruments, including ToF-SIMS, SEM, and NMR, allowing chemical insight into the complex l-l interface. This project studies the l-l interactions at the molecular level and provide unprecedented insight into the physicochemical processes of bilgewater emulsions.

SERDP-recommended emulsion systems were used as the base models for synthetic bilgewater studies. Specifically, synthetic bilgewater is similar to MEPC 107(49) test fluid C emulsion [16]. More importantly, real bilgewater samples as well as a NSWC Carderock surrogate sample from SERDP funded labs were shared and studied in this project complementing other ongoing bilgewater emulsion research. Emulsions prepared by mechanical means were used to serve as the surrogate and be analyzed using multiple imaging techniques to understand their surface properties, size, morphology, aggregation, and l-l interactions.

Besides bulk approaches to study emulsions, the unique multiplexed chemical imaging capability has been employed to decipher the complex interfacial process in emulsion formation, breaking, and separation. Specifically, our approach can capture the l-l interface and study how stressors [6, 11, 12, 18-20] (e.g., biofouling, particulate, and salinity) affect emulsion formation and transformation. Two tasks were performed. Task 1 aims to establish feasibility of multimodal imaging applications to study bilgewater emulsions and demonstrate how different measurement results can be integrated to understand the l-l interface transformation. Task 2 builds upon our expertise in biofilm imaging and optimal bilgewater analysis conditions to be obtained in Task 1 to investigate the effect of microbes on bilgewater stabilization or breaking. These initial results will set the technical and scientific foundations for further systematic studies of bilgewater stabilization, breaking, and mitigation. In addition, project management, reporting, and manuscript preparation were performed corresponding to each task.

4.1 Task 1 Bilgewater multimodal imaging

The presence of a native or added surfactant is necessary for the long-term stability of emulsions: the surfactant molecules migrate to the l-l interface and inhibit droplet coalescence. The synthetic bilgewater and real bilgewater samples were studied to understand how factors such as ionic, nonionic surfactant micelles, or solid affect emulsion stabilization in situ. In situ multiplexed imaging tools including SIMS, SEM, or NMR were used. The same sample can be transferred among these instrument platforms via our unique microfluidic reactor. Synthetic bilgewater emulsion samples were used to establish suitable imaging conditions followed with analysis of real bilgewater samples.

Correlative imaging offers a great deal of information and provide a more holistic view of the complex system. First the bilgewater droplet size distribution (DSD) was determined using NMR and SEM. NMR, particularly, pulsed-field gradient (PFG), has long been used in emulsion studies.[1, 2] Emulsion formation, droplet cluster structure, diffusion in the liquid, and velocity distributions in a confined field have been reported using NMR measurements.[1-9] These approaches were used to obtain an overview of the bilgewater DSD), diffusion, and velocity distribution. Such information is useful to characterize the emulsion inside the microchannel, providing the physical measurements for future computational fluid dynamic (CFD) simulation. By complementing with other imaging studies, more complete pictures of the emulsion stabilization can be achieved. However, in the NMR measurements, the operator used the wrong pulse sequence and did not obtain the desirable results in the initial trial. Due to limited funding and time, we did not pursue additional measurements. It is possible that the PFG measurements are doable to obtain usable parameters for bilge emulsions. We plan to pursue this subtask if permitted with additional funding.

We prepared and published a paper to report the first ToF-SIMS imaging and analysis of bilge emulsion in Chemosphere [10]. More details are provided in Appendix A. This paper establishes the technical soundness for using ToF-SIMS to study bilge emulsions.

In addition, in situ liquid SIMS, a new technique developed in my group at PNNL, was used to provide submicron-resolution molecular mapping of the liquid surface and interface in bilgewater emulsion.

4.1.1 In situ SEM imaging of bilge emulsion

More importantly, in situ SEM imaging in the high vacuum mode, a new technique developed in our lab, was used to determine DSD. Figs. 1a & 1b shows the SEM images a fresh and aged bilge emulsions, respectively.

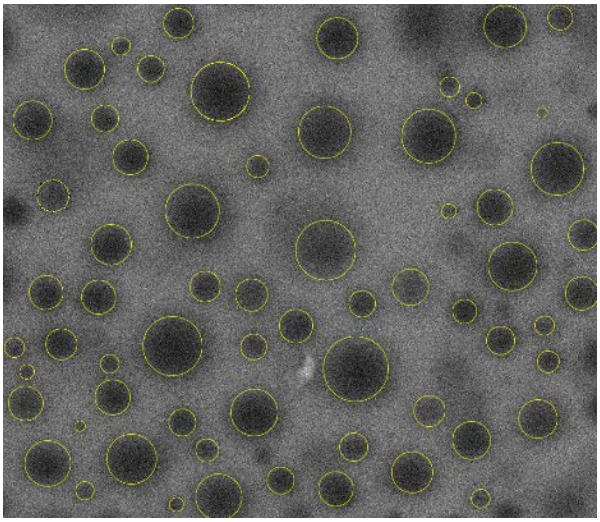

FIG. 1a. In situ SEM imaging of fresh bilge emulsion.

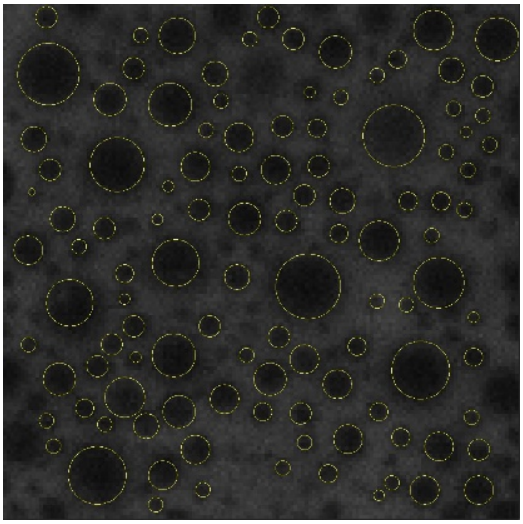

FIG. 1b. In situ SEM imaging of aged bilge emulsion.

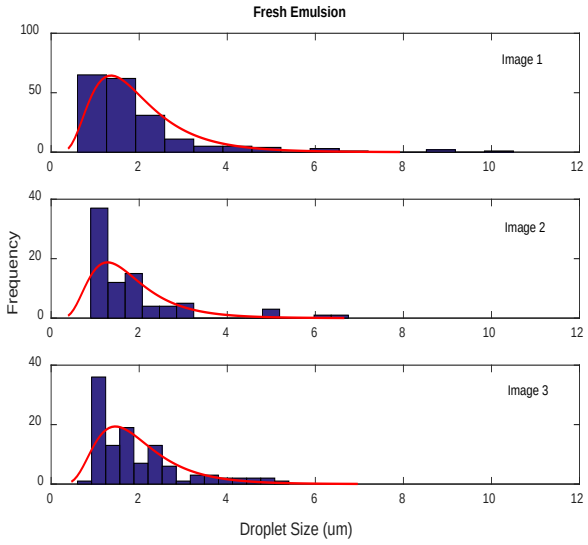

FIG. 2a. DSD of fresh bilge emulsion by in situ SEM.

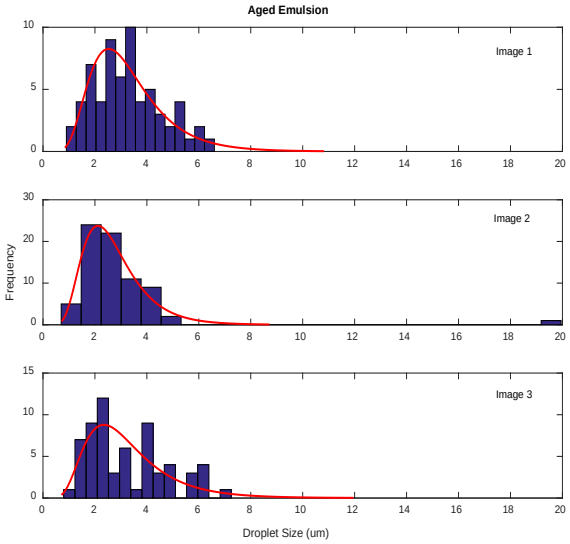

FIG. 2b. DSD of aged bilge emulsion by in situ SEM.

Figs. 2a and 2b depict size determination of fresh and aged bilge emulsions. Compared to the only other wet commercial SEM device, we can provide both SE and BSE images and give information on particle size, shape, and morphology. This novel technique was successfully used to characterize bilge emulsion DSD in the limited scope project. Elemental mapping by EDX gives more insight into the chemical distribution on the particle surface. This kind of measurement will be useful to understand how solid emulsifiers stabilize the emulsion droplets.

We certainly are interested in pursuing additional measurements and observations of bilge compositions in relation to DSD in the next stage of this project.

4.1.2 In situ liquid SIMS imaging of bilge emulsion

In preparation to fully understand the liquid SIMS data, we studied the dry bilge emulsions and components using statics SIMS and complemented the chemical measurements using optical microscopy to determine DSD. This step is important in defining reference spectra in liquid SIMS data interpretation. A manuscript was submitted to Chemosphere, and it is published in July 2019. The published version of the manuscript is attached in Appendix A to show progress of this task.

In the first paper reporting ToF-SIMS imaging and analysis of bilge emulsion, we used a Navy model and determine DSD using optical microscopy. Our findings suggest that the aged emulsion not only grows in size but also has significant surface compositional changes. Both oil and detergent components appear in the emulsion surface as soon as fresh droplets form as expected. Higher mass organics from the surfactant components appear at the droplet surface as droplets age. Surface oxidation is another factor that modifies the emulsion chemical makeup over time, however, this effect is not significant. This is probably because the samples were prepared in a well-controlled nitrogen drying environment. Drying has an effect on the emulsion analysis results. One of the most significant effect is loss of the water phase. Although we can map oil and detergent components using the ToF-SIMS mass spectrometry imaging of dry emulsion samples, it is not possible to study the water phase in the O/W emulsion using static SIMS. Therefore, in situ liquid SIMS was deployed to probe the dynamic oil-water liquid-liquid phase evolution in this task as well.

4.1.2.1 Experimental setup

The same procedure used in previous synthetic bilgewater generation studies have been adapted to study the emulsion surface changes in this work [11]. The synthetic emulsion sample consisted of a liquid mixture of 10 mL Navy Standard Bilge Mix (NSBM) #4 abbreviated as oil mix herein and 1 mL of detergent mix. The oil mix consists of 50% diesel fuel marine (MIL-PRF-16884N), 25% 2190 TEP steam lube oil (MIL-PRF-17331K), and 25% 9250 diesel lube oil (MIL-PRF-9000L). The detergent mix consisted of 50% type 1 general purpose detergent (MIL-D-16791G (1)), 25% commercial detergent Tide Ultra (liquid), and 25% degreasing solvent (MIL-PRF-680C, Type III). The oil mix and detergent mix were provided by the collaborators at the Naval Surface Warfare Center, Carderock Division.

The details of SALVI microfluidic reactor fabrication were reported in previous papers. [3, 5, 6, 8-15]

The mass spectral and image measurements were conducted on a ToF-SIMS 5 instrument (IONTOF GmbH, Münster, Germany). The liquid was sealed in a SALVI device underneath a 100 nm thick SiN membrane. The primary ion beam was a 25 keV Bi_3^+ primary ion beam. Dynamic profiling drilled an aperture with 2 µm in diameter through the SiN membrane. The liquid in the microchannel membrane was withheld by its surface tension across the aperture.[12, 13] Secondary ions could be then emitted at an energy range of 0 to 10 eV from the aperture. More experimental details are described in our previous publications.[14, 15]

The liquid SIMS mass spectral data was processed using the IONTOF Surface Lab 6.3 software. The mass spectra were calibrated by OH^- (m/z$^-$ 17), $SiC_2H_5O^-$ (73), $Si_2C_3H_9O_3^-$ (m/z$^-$ 149), $Si_3C_5H_{15}O_4^-$ (m/z$^-$ 223) in the negative mode; and CH_3^+ (m/z$^+$ 15), $(CH)_3Si^+$ (m/z$^+$ 73), $Si_2OC_5H_{15}^+$ (m/z$^+$ 147), $Si_3C_5H_{15}O_3^+$ (m/z$^+$ 207), $Si_4O_4C_7H_{21}^+$ (m/z$^+$ 281) in the positive mode, respectively. Spectral principal component analysis (PCA) was conducted using the MATLAB R2014a software (MathWorks, Natick, Massachusetts). For the first round of PCA, known interference peaks were removed, including m/z$^-$ 1 H^-, m/z$^-$ 12 CH^-, m/z$^-$ 16 O^-, m/z$^-$ 24 C_2^-, m/z$^-$ 25 C_2H^-, m/z$^-$ 28 Si^-, m/z$^-$ 29 SiH^-, m/z$^-$ 41 $SiCH^-$, m/z$^-$ $SiCH_2^-$, m/z$^-$ 44 SiO^-, m/z$^-$ 45 $SiOH^-$, m/z$^-$

58 $SiCH_2O^-$, m/z$^-$ 59 $SiCH_3O^-$, m/z$^-$ 60 SiO_2^-, m/z$^-$ 73 $SiC_2H_5O^-$, m/z$^-$ 75 $SiCH_3O_2^-$, m/z$^-$ 149 $Si_2C_3H_9O_3^-$, m/z$^-$ 163 $Si_2C_5H_{15}O_2^-$, m/z$^-$ 223 $Si_{13}C_5H_{15}O_4^-$, and m/z$^-$ 237 $Si_3C_7H_{21}O_3^-$ in the negative mode and m/z$^+$ 28 Si^+, m/z$^+$ 59 CH_3SiO^+, m/z$^+$ 73 $(CH_3)_3Si^+$, m/z$^+$ 147 $Si_2O_5H_{15}^+$, m/z$^+$ 207 $Si_3C_5H_{15}O_3^+$, m/z$^+$ 281 $Si_4O_4C_7H_{21}^+$, m/z$^+$ 369 $Si_5O_4C_{11}H_{33}^+$, m/z$^+$ 209 Bi^+, m/z$^+$ 418 Bi_2^+, and m/z$^+$ 657 Bi_3^+ in the positive ion mode. For the second round of PCA, peaks were selected according to the following criteria: a) the intensity of the peak in the SIMS mass spectrum was significantly higher than its neighboring peaks, b) peaks identified in dry sample analysis or other relevant publications (e.g., [10]), c) water clusters, and d) peaks in the SIMS mass spectrum bigger than m/z$^+$ 40 or m/z$^-$ 40. Before performing PCA, raw data were treated by normalization to the total selected peak intensity, square-root transformation, and mean centering.

4.1.2.2 Spectral comparison of in situ liquid SIMS imaging of bilge

Table 1 gives the sample matrix of the bilge emulsion using in situ liquid SIMS. These analyses were completed in the limited scope project.

Sample ID	Description	Status
Fresh bilge	Emulsion generated with NSBM #4 and DM sample no dilution at 3500 rpm	Done
Aged bilge	Emulsion generated with NSBM #4 and DM sample no dilution at 3500 rpm	Done
Oil mix	50% NSBM 4-1 + 25% NSBM 4-2 + 25% NSBM 4-3	Done
Detergent mix	50% DM1 + 25% DM2 +25% DM3	Done
Fresh bilge & X-100	Fresh emulsion and X-100 (1:1) vortexed for 1 min	Done
Di water	DI water as the solvent for O/W emulsion	Done

Table 1. Sample matrix of in situ liquid SIMS analysis of bilge emulsions

Fig. 3 shows SIMS spectral comparison showing the two important liquid phase oil and water with complex composition. This result demonstrates that the l-l interface can be spatially mapped using liquid SIMS. We are continuing the liquid SIMS analysis and will be preparing for a second manuscript to report scientific findings that are mapped at the l-l interface showing different chemical distribution in bilgewater emulsions, differentiating the oil and water phases in space at the submicrometer scale. Such knowledge is needed to map the oil-water interface encountered in bilgewater emulsions.

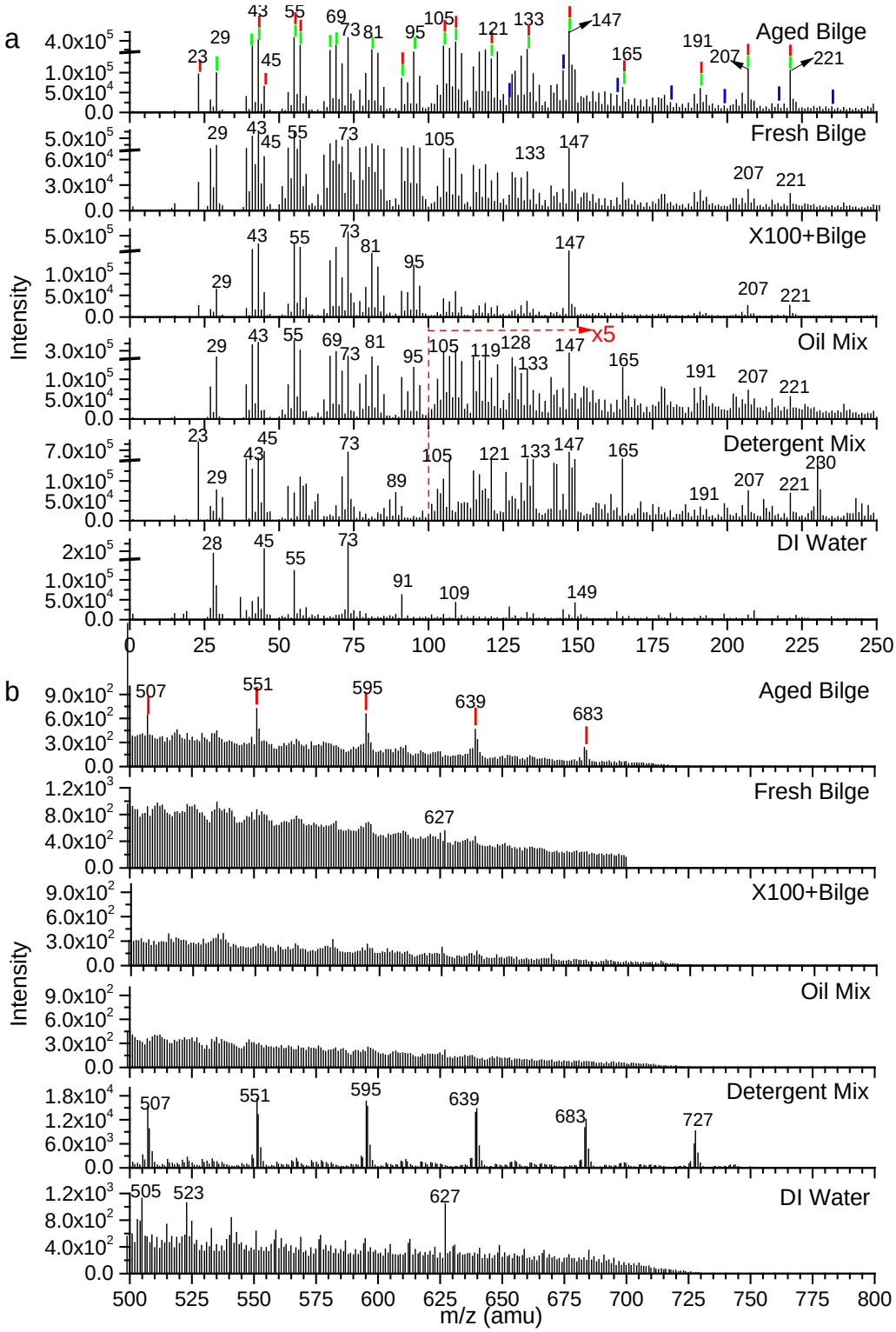

FIG. 3. In situ liquid SIMS spectral comparison of aged bilge, fresh bilge, X100 and bilge, oil mix, detergent mix, and DI water in the mass range 1-250 (a) and 500-800.

Additional spectral results will be presented in our second manuscript reporting findings of the oil-water liquid-liquid interfacial changes between the fresh and aged bilge emulsion.

4.1.2.3 SIMS Spectral PCA of in situ liquid SIMS analysis of bilge

We conducted spectral PCA of the in situ liquid SIMS data set. Fig. 4 depict representative PCA scores plots and loadings plots in the negative ion mode.

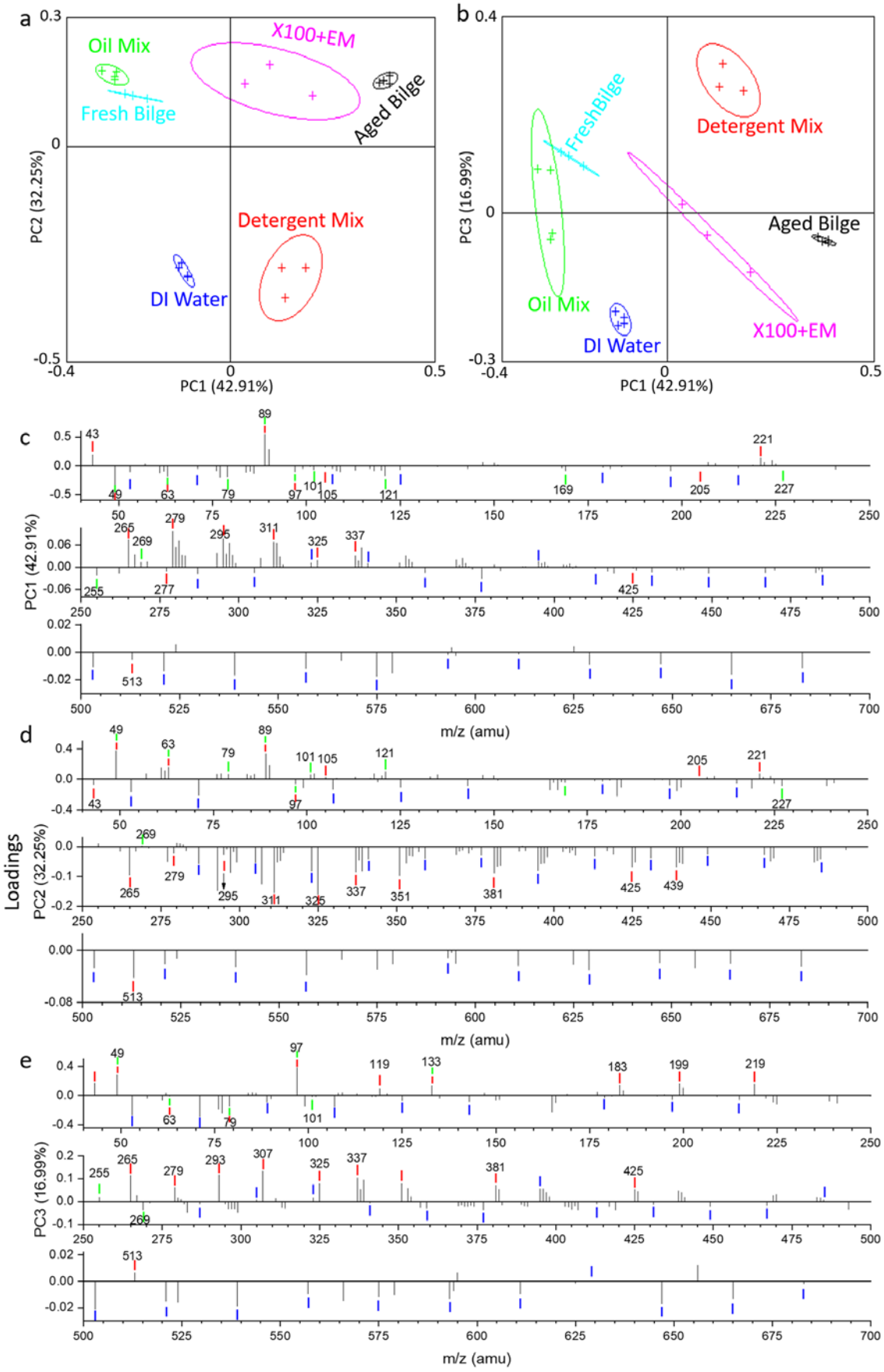

FIG. 4. In situ liquid SIMS spectral PCA results: a) PC1 vs. PC2 scores plot; b) PC1 vs. PC3 scores plot; c) PC1; d) PC2; and e) PC3 loadings plots in the negative ion mode.

In the negative mode, principal components (PC1, PC2 and PC3) explain 92.15% of all data. PC1 explain 42.91% of data and mainly separates the DI water control, oil mix and fresh bilge from aged bilge and detergent mix. It's not surprising that the sample consisting of X-100 and fresh bilge exists between PC1 positive and negative, nicely positioned between the detergent and bilge emulsions. PC2 explains 32.25% of data and it mainly separates the detergent mix and DI water from aged bilge, fresh bilge, and oil mix and detergent mix. PC3 explains 16.99% of all data and it mainly separates the fresh bilge and detergent mix from aged emulsion and DI water.

In PC1 negative mode loading, oil mix, fresh bilge and water cluster are the main contributors. Oil mix peaks, such as m/z $^-$ 49 C_4H^-, 63 C_5H_3-, 79 $C_6H_7^-$ and water clusters, such as m/z$^-$ $(H_2O)_nOH^-$, n=2, 3, 5, 6, 7, 9, 10, 11, make great contributions to the formation of fresh bilge. PC1 positive separates aged bilge emulsion and detergent mix from fresh bilge emulsion and oil mix. This finding suggests that the bilge surface change over time, and that detergent components have higher contribution to the aged emulsion. Some detergent peaks, especially in the high mass range, identified as m/z$^-$ 325, 337, only exist in aged bilge but not in fresh bilge. This means that these detergent components do not appear immediately in the fresh bilge surface; instead they show up in the aged bilge surface as time goes. This finding confirms the chemical surface change of O/W bilgewater droplets over time using static SIMS. PC2 positive scores plot shows oil mix, fresh bilge, aged bilge and X-100+fresh bilge share similar features. This finding suggests some oil components, such as m/z$^-$ 49 C_4H^-, 63 $C_5H_3^-$, 79 $C_6H_7^-$ and detergent components, such as m/z$^-$ 101, 105, 205, 221, show up immediately in the fresh bilge and persist in aged bilge over time.

In PC3 positive, oil and detergent components share same peaks, and both contribute to fresh bilge and X100 and fresh bilge. Some characteristic peaks include m/z$^-$ 49 C_4H^-, 205, 425, and 513. PC3 negative separates aged bilge and DI water from fresh emulsion and detergent mix, which further confirms that the bilge surface change over time. In addition, water clusters, such as m/z$^-$ $(H_2O)_nOH^-$, n= 3,4,5,6,7,9,10,11, make contributions the aged bilge. The sample consisting of X-100 and fresh bilge share common peaks with fresh and aged bilge. Overall, the observation of water clusters in both fresh and aged bilge indicates that water clusters play an important role in the formation of bilge. In addition, we observe bilge surface change over time. Detergent components, especially those high mass peaks only show up in the aged bilge but not in the fresh bilge, providing another evidence of bilge surface compositional change.

A manuscript is being prepared to report the key findings of the evolved oil-water interface using in situ liquid SEM and in situ liquid SIMS. In situ NMR analysis was also conducted to determine the diffusion constant and cluster size in the bilge emulsion. More details are provided in Appendix B.

4.1.3 Bilge evolution in both droplet size and surface chemical composition

Both static ToF-SIMS and dynamic ToF-SIMS surface analysis indicate that the bilge surface chemical composition changes comparing between fresh and aged emulsions. In addition, droplet size evolves over time. Both optical and in situ SEM DSD results show that the droplet size increases over time. Fig. 5 illustrates the conceptual understanding of the interfacial change of bilgewater using the unique imaging approaches in this project

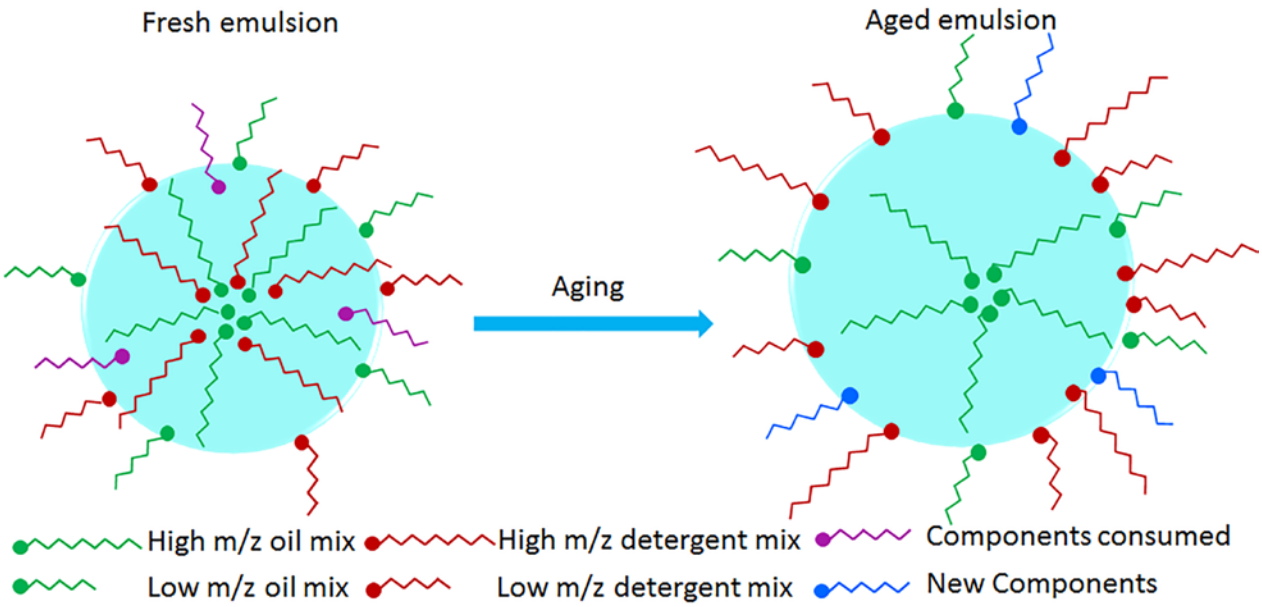

FIG. 5. The evolving oil-water bilgewater emulsion interface [10].

4.2 Task 2 Bilgewater and biofilm interactions

Microorganisms may influence the formation and stabilization of emulsions by producing surfactants, altering the chemistry and pH of bilgewater, and scavenging available oxygen and thus limiting the oxidative decomposition of oil and surfactants. Cells and cell fragments could also help form oil particle aggregates (OPAs), which are very stable and do not readily coalesce.[16-19] The presence of higher concentrations of cells and cellular exudates are suspected to change the viscosity and salinity of bilgewater, further enhancing the emulsion stability. Some microorganisms may also contribute to the breakdown of emulsions by metabolizing the oil or scavenging the biological surfactants as a carbon and energy source. All microorganisms produce a variety of amphiphilic molecules that act as biological surfactants to help emulsify oil.[20-22] These surfactants may be summarized in four categories: glycolipids, fatty acids, lipoproteins, and polymers.[23-27] *Mannosylerythritol* lipids (MELs), a glycolipid, are powerful surfactants capable of reducing aqueous surface tension to ~25.1 mN/m.[27] Microbial metabolism, particularly in iron oxide rich and reduced oxygen water, results in the production of biological acids, which may lower the pH of bilgewater. Cells sequester water from the surrounding environment and are adept at maintaining concentration differentials. For instance, hydrophobic bacteria was found to stabilize O/W emulsions,[28] however, little is known about how microbes including biofilms affect bilgewater emulsion formation and degradation.

Microbes essentially have two general means of interacting with an emulsion: through direct whole-cell contact with the dispersed phase or through indirect influence via biochemistry that the cells release into the continuous phase through normal metabolism or as a consequence of processes (e.g., chemical disruption of membranes or sheering) that lyse the cells.[29, 30] Additionally, cells and cellular bodies may be found in one of four phases in bilgewater: biofilms, the surface microlayer, planktonic cells, or larger flocculating clusters, each possessing unique communities and behaviors. This task was used to examine the effects of viable cells and cell-derived biochemistry on emulsification and stability in bilgewater.

4.2.1 Culture selected microbes in the microfluidic reactor

4.2.1.1 Sample matrix

Table 2 gives the sample matrix of the bilge emulsion using the SALVI microreactor for biofilm culture and ToF-SIMS for analysis. These analyses were completed in the limited scope project.

No.	Bacteria	Description	Status	Priority	Goal
1	Pseudomonas (P)	Planktonic cells	Done	√	Phase I
2		Biofilms	Done	√	Phase I
3		Growth media	Done	√	Phase I
4		Growth media with emulsion	Done	√	Phase I
5	Arthrobacter (A)	Planktonic cells	Done	√	Phase I
6		Biofilms	Done	√	Phase I
7		Growth media	Done	√	Phase I
8		Growth media with emulsion	Done	√	Phase I
9	Cobetia marina (C)	Planktonic cells	TBD		Phase II
10		Biofilms	TBD		Phase II
11		Growth media	TBD		Phase II
12		Growth media with emulsion	TBD		Phase II

Table 2. Sample matrix of biofilm and bilge emulsion interactions

4.2.1.2 Growth curve

The growth curves of each biofilm were established prior to any bilge and biofilm interaction experiments. Details of these growth curves are necessary in the biofilm culture and they will be reported in our manuscript reporting the biofilm and bilgewater interactions. Preliminary findings were reported in SEMS in a previous quarterly report.

4.2.2 Study microbial biofilm effects on real bilgewater emulsions using advanced imaging

4.2.2.1 Experimental setup

The objective of this experiment was to compare chemical changes between biofilm and bilgewater exposed to biofilm. Pseudomonas fluorescens and Arthrobacter bacteria species were selected and cultured to form biofilms in the microchannel within a SALVI microfluidic reactor. Before culturing biofilm in a SALVI, each bacteria organism was cultured on agar plates for 24 hrs. from frozen stocks. Then cultured bacteria was inoculated in 20 mL of fresh LB medium contained in a 50 mL plastic tubes for 24 hr. incubation. The incubation condition was 35 °C in a shaker with a rate of 150 rpm.

The incubated bacteria planktonic cell (10 mL) was injected into the SALVI setup illustrated in Fig. 6 at a flow rate of 2 µL/min. After bacteria incubated media was injected to generate biofilm within the SALVI channel, fresh medium was injected at 2 µL/min continuously. The fresh medium injection and continued culture have been done in room temperature for three days.

After each organism's biofilms within the SALVI microchannel had fully grown, the control biofilm samples were collected in a tube at the end of the SALVI setup.

To expose bilgewater into fully grown biofilms, a 1:1 (fresh medium to bilgewater) medium mixture was injected into the SALVI setup at 2 µL/min (Fig. 6). Bilgewater exposed biofilms were collected from the collection tube after 24 hours, and this is the day 1 biofilm and bilge interaction sample. After 48 hours another set of bilgewater exposed biofilm samples were

collected in the same manner (or day 2 biofilm and bilge interaction sample). This set of samples were used to study the effect of biofilms on bilge emulsions over time.

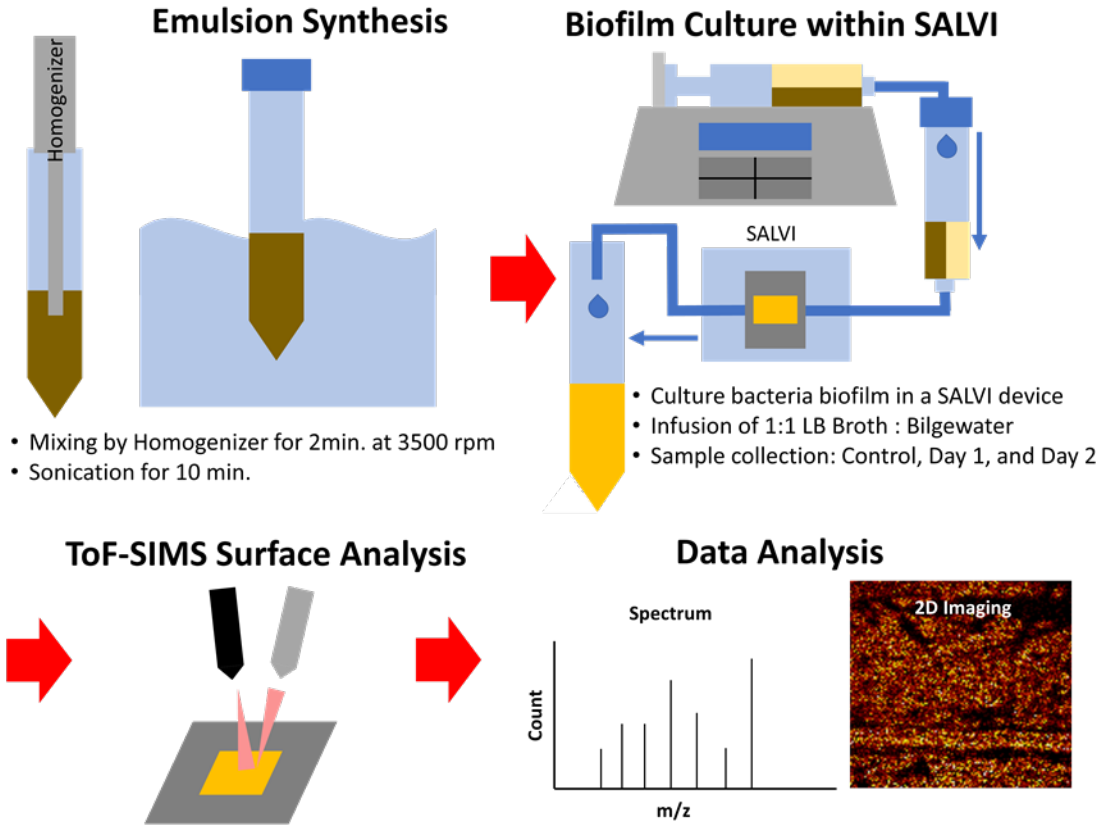

FIG. 6. Schematic showing biofilm and bilge interaction experimental setup and sample collection.

The collected biofilms were placed on clean Si chips and dried in a biosafety cabinet (BSC) for a couple of hours. Dried samples including LB media, control biofilms, bilge and biofilm mixture at day 1, and day 2) were loaded into ToF-SIMS for surface analysis. Similar to Task 1, it is important to establish mass spectra with high mass accuracy using static SIMS before employing dynamic SIMS to study the liquid biofilm and bilge mixtures. We fully intend and plan to continue task 2 and study the biofilm effect using in situ imaging tools permitted by additional funding.

4.2.3 ToF-SIMS spectral analysis and comparison

Fig. 7 depicts SIMS spectral comparison of fresh bilge, LB broth, P. and bilge collected at day 2, P. and bilge collected at day 1, and P. biofilm in the mass range 1-250 (a) and 250-500 (b) in the positive ion mode. P. is the abbreviation of Pseudomonas. SIMS spectra show different features for biofilms and bilgewater emulsions that have interacted with P. biofilm over different periods of time. SIMS spectral features suggest time has an effect on the bilge and biofilm interactions. This set of results is under further investigation to identify interesting peaks of relevance to biofilms and bilge components. These results will be presented in a third manuscript.

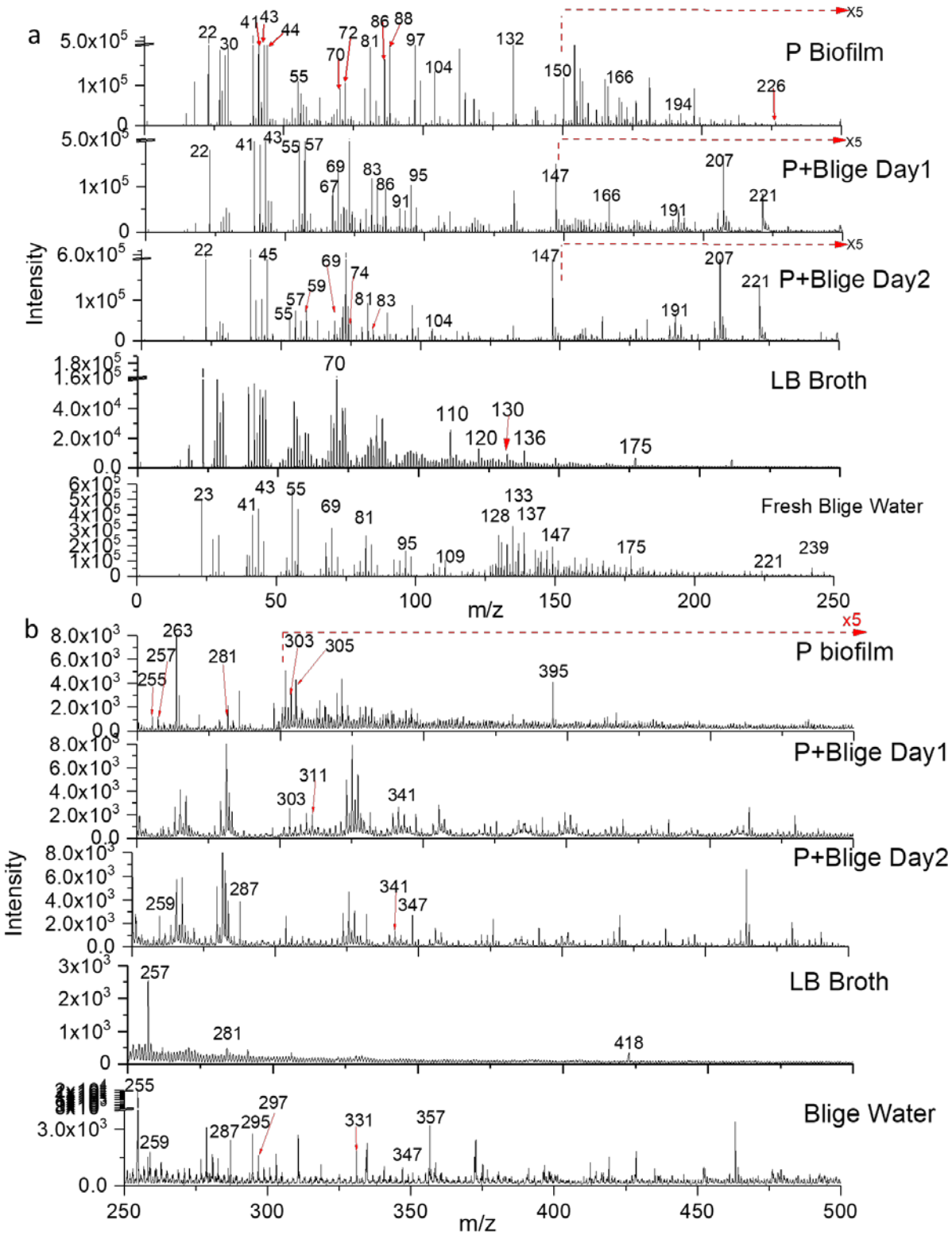

FIG. 7. ToF-SIMS spectral comparison of fresh bilge, LB broth, P. and bilge collected at day 2, P. and bilge collected at day 1, and P. biofilm in the mass range 1-250 (a) and 250-500 (b) in the positive ion mode. P. is the abbreviation of Pseudomonas.

4.2.4 Initial ToF-SIMS spectral PCA results of biofilms effects on bilge

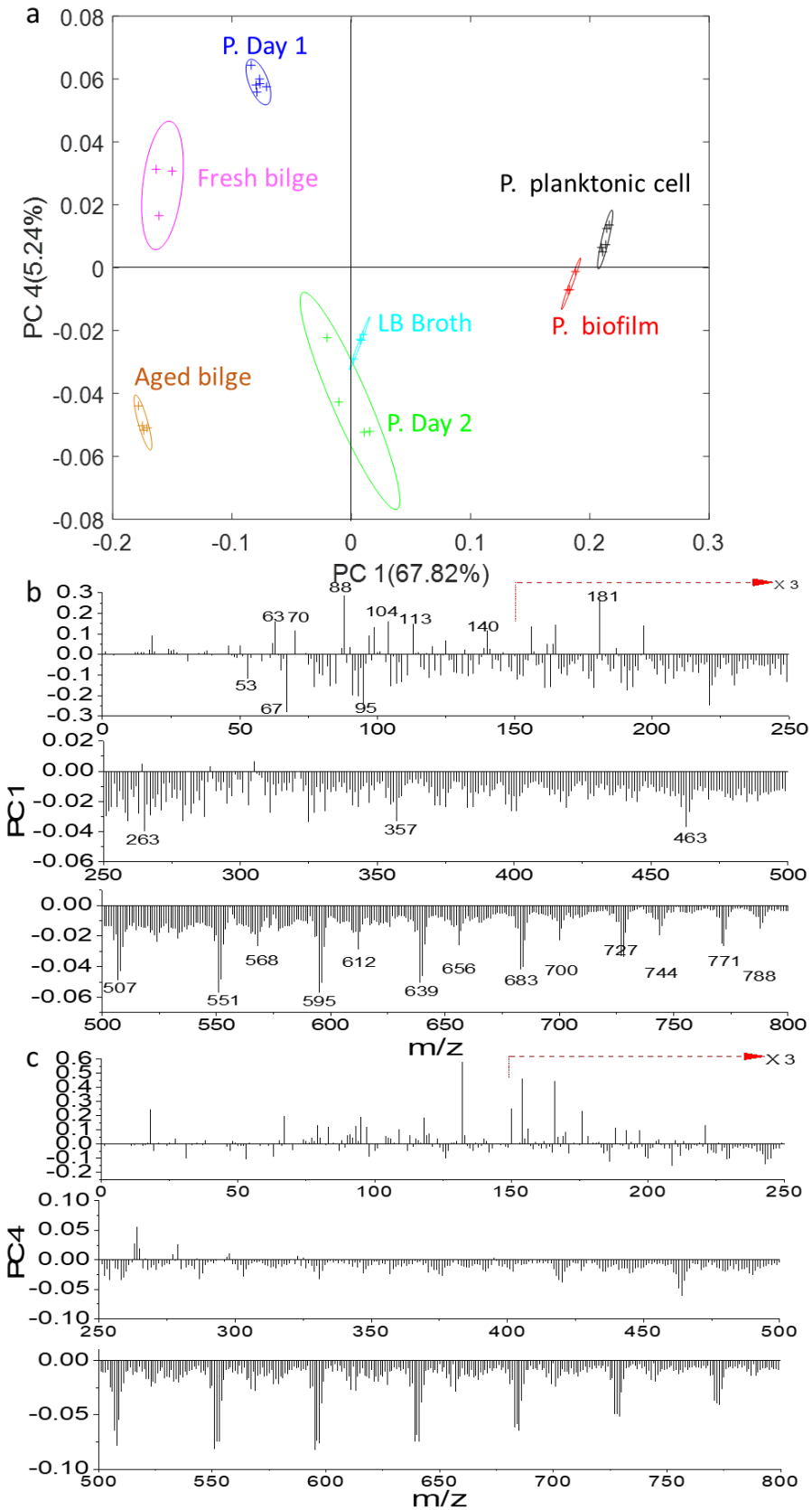

FIG. 8. ToF-SIMS spectral PCA results: a) PC1 vs. PC4 scores plot; b) PC2 vs. PC4 scores plot; c) PC1; d) PC2; and e) PC4 loadings plots in the positive ion mode.

Because of the nature of SIMS spectra and Poisson noise, PCA is considered a good approach to decode its complexity. Fig. 8 depicts representative spectral PCA results including PC1 vs. PC4 scores and loadings plots in the positive ion mode.

Specifically, PC1 separates P. biofilm and planktonic cell from the fresh/aged bilge and bilge emulsions exposed to biofilms. PC4 separates the fresh and aged bilge and the bilge exposed to biofilms over different times. Fresh bilge emulsion and bilge treated with biofilm for one day are more similar (PC4 positive) compared to aged bilge and bilge treated with biofilm for two days (PC4 negative). The similarity between planktonic cells and bilge interacted with biofilm over one day suggests that the initial effect may come more from the planktonic cells than the biofilms in day 1, which is supported by PC4 positive and associated loadings. In day 2, the biofilm itself would exert more effect on the bilge as evidenced by loadings and similar scores in PC4 negative. We are working on additional analysis and we plan to summarize findings in a third manuscript.

5.0 Summary and Recommendations

We successfully accomplished the proposed technical tasks in the limited SERDP project WP 18-1660. We demonstrated that the in situ correlative imaging of bilge emulsion is possible using the advance chemical imaging techniques such as SEM and ToF-SIMS. We present two key results in task 1. First of all, droplet size distribution of bilge emulsion seems to grow from fresh to aged particles in water based on optical and in situ SEM imaging. Moreover, unique oil and water interfacial information and evolution can be captured using in situ liquid SIMS. In task 2, we illustrated that biofilm effects on bilge could be probed using ToF-SIMS. We also find that both planktonic cells and biofilms have an effect on the oil-in-water bilge changes.

To continue this research using advanced imaging techniques to understand bilge formation, stabilization and breaking to establish more efficient wastewater treatment strategies, we recommend the following,

1. Continue collaboration with NAVY and use the same bilge model developed by NAVY

2. Develop a droplet SALVI microreactor to permit in operando chemical imaging of oil-in-water bilge formation, stabilization, and breaking using in situ SEM and in situ SIMS

3. Expand and optimize in situ PFG NMR to complement bilge droplet size distribution

4. Study the effect of surfactants on bilge using the in operando E-cell and build the technical base for novel bilge separation

5. Investigate biofilm effects on bilge evolution further using in situ optical imaging and in situ SIMS chemical imaging

We anticipate to obtain more fundamental understanding of the bilge stabilization and breaking. More systematic conditions can be studied using the above approaches. Such information is critical to develop new mitigation techniques or strategies for wastewater treatment of importance to SERDP. The limited scope project generates sufficient results for three manuscripts. One paper is already published, and two papers are in preparation. We also trained a post bachelor research assistant, a graduate student, and a recent postdoctoral research assistant in the process of this work.

6.0 References

1. M. L. Johns, NMR studies of emulsions. Current Opinion in Colloid & Interface Science 2009, 14, (3), 178-183.

2. R. Bernewitz; Guthausen, G.; Schuchmann, H. P., NMR on emulsions: characterisation of liquid dispersed systems. Magn. Reson. Chem. 2011, 49, S93-S104.

3. C. P. Aichele; Chapman, W. G.; Rhyne, L. D.; Subramani, H. J.; House, W. V., Analysis of Formation of Water-in-Oil Emulsions. Energy Fuels 2009, 23, (7), 3674-3680.

4. R. Bernewitz; Dalitz, F.; Kohler, K.; Schuchmann, H. P.; Guthausen, G., Characterisation of multiple emulsions by NMR spectroscopy and diffusometry. Microporous and Mesoporous Materials 2013, 178, 69-73.

5. R. Bernewitz; Schmidt, U. S.; Schuchmann, H. P.; Guthausen, G., Structure of and diffusion in O/W/O double emulsions by CLSM and NMR-comparison with W/O/W. Colloid Surf. A-Physicochem. Eng. Asp. 2014, 458, 10-18.

6. M. L. Johns; Gladden, L. F., Sizing of emulsion droplets under flow using flow-compensating NMR-PFG techniques. J. Magn. Reson. 2002, 154, (1), 142-145.

7. J. Kang; Guo, Q.; Phillips, G. O.; Cui, S. W., Understanding the structure-emulsification relationship of gum ghatti - A review of recent advances. Food Hydrocolloids 2014, 42, 187-195.

8. G. H. Sorland, Characterization of Emulsions by PFG-NMR. In Magnetic Resonance in Porous Media, Fantazzini, P.; Bortolotti, V.; Karger, J.; Galvosas, P., Eds. Amer Inst Physics: Melville, 2011; Vol. 1330, pp 27-30.

9. M. A. Voda; van Duynhoven, J., Characterization of food emulsions by PFG NMR. Trends Food Sci. Technol. 2009, 20, (11-12), 533-543.

10. J. Son; Shen, Y.; Yao, J.; Paynter, D.; Yu, X.-Y., Surface evolution of synthetic bilgewater emulsion. Chemosphere 2019, 236, 124345.

11. J. Church; Paynter, D. M.; Lee, W. H., In situ characterization of oil-in-water emulsions stabilized by surfactant and salt using microsensors. Langmuir 2017, 33, (38), 9731-9739.

12. X. Hua; Szymanski, C.; Wang, Z.; Zhou, Y.; Ma, X.; Yu, J.; Evans, J.; Orr, G.; Liu, S.; Zhu, Z., Chemical imaging of molecular changes in a hydrated single cell by dynamic secondary ion mass spectrometry and super-resolution microscopy. Integr. Biol. 2016, 8, (5), 635-644.

13. J. Yu; Zhou, Y.; Hua, X.; Zhu, Z.; Yu, X.-Y., In situ characterization of hydrated proteins in water by SALVI and ToF-SIMS. JOVE J. Vis. Exp. 2016, (108), e53708-e53708.

14. X. Sui; Zhou, Y.; Zhang, F.; Chen, J. M.; Zhu, Z.; Yu, X.-Y., Deciphering the Aqueous Chemistry of Glyoxal Oxidation with Hydrogen Peroxide Using Molecular Imaging. Phys. Chem. Chem. Phys. 2017, 19, (31), 20357-20366.

15. X. Sui; Zhou, Y.; Zhang, F.; Zhang, Y.; Chen, J.; Zhu, Z.; Yu, X.-Y., ToF-SIMS characterization of glyoxal surface oxidation products by hydrogen peroxide: a comparison between dry and liquid samples. Surf. Interface Anal. 2018, 50, (10), 927-938.

16. L. Zhao; Boufadel, M. C.; Geng, X.; Lee, K.; King, T.; Robinson, B.; Fitzpatrick, F., A-DROP: A predictive model for the formation of oil particle aggregates (OPAs). Marine Pollution Bulletin 2016, 106, (1–2), 245-259.

17. R. Aveyard; Binks, B. P.; Clint, J. H., Emulsions stabilised solely by colloidal particles. Adv. Colloid Interface Sci. 2003, 100–102, 503-546.

18. L. O. Ajijolaiya; Hill, P. S.; Khelifa, A.; Islam, R. M.; Lee, K., Laboratory investigation of the effects of mineral size and concentration on the formation of oil–mineral aggregates. Marine Pollution Bulletin 2006, 52, (8), 920-927.

19. Y. Gong; Zhao, X.; Cai, Z.; O'Reilly, S. E.; Hao, X.; Zhao, D., A review of oil, dispersed oil and sediment interactions in the aquatic environment: Influence on the fate, transport and remediation of oil spills. Marine Pollution Bulletin 2014, 79, (1–2), 16-33.

20. J. Komaiko; Sastrosubroto, A.; McClements, D. J., Formation of Oil-in-Water Emulsions from Natural Emulsifiers Using Spontaneous Emulsification: Sunflower Phospholipids. J. Agric. Food Chem. 2015, 63, (45), 10078-10088.

21. J. Qiu, Stability of the Oil-water Emulsion Formed During Amphiphilic Polymer Flooding. Petroleum Science and Technology 2013, 31, (2), 142-147.

22. J. E. Zajic; Supplisson, B.; Volesky, B., Bacterial degradation and emulsification of No. 6 fuel oil. Environ. Sci. Technol. 1974, 8, (7), 664-668.

23. D. Kitamoto; Morita, T.; Fukuoka, T.; Konishi, M.-a.; Imura, T., Self-assembling properties of glycolipid biosurfactants and their potential applications. Current Opinion in Colloid & Interface Science 2009, 14, (5), 315-328.

24. M. Ongena; Jacques, P., Bacillus lipopeptides: versatile weapons for plant disease biocontrol. Trends Microbiol. 2008, 16, (3), 115-125.

25. D. Kitamoto; Isoda, H.; Nakahara, T., Functions and potential applications of glycolipid biosurfactants — from energy-saving materials to gene delivery carriers —. J. Biosci. Bioeng. 2002, 94, (3), 187-201.

26. S. Lang, Biological amphiphiles (microbial biosurfactants). Current Opinion in Colloid & Interface Science 2002, 7, (1–2), 12-20.

27. J. I. Arutchelvi; Bhaduri, S.; Uppara, P. V.; Doble, M., Mannosylerythritol lipids: a review. J. Ind. Microbiol. Biotechnol. 2008, 35, (12), 1559-1570.

28. L. S. Dorobantu; Yeung, A. K. C.; Foght, J. M.; Gray, M. R., Stabilization of Oil-Water Emulsions by Hydrophobic Bacteria. Appl. Environ. Microbiol. 2004, 70, (10), 6333-6336.

29. J. Park; Jeters, R. T.; Kuo, L.-J.; Strivens, J. E.; Gill, G. A.; Schlafer, N. J.; Bonheyo, G. T., Potential Impact of Seawater Uranium Extraction on Marine Life. Ind. Eng. Chem. Res. 2016, 55, (15), 4278-4284.

30. J. Park; Gill, G. A.; Strivens, J. E.; Kuo, L.-J.; Jeters, R. T.; Avila, A.; Wood, J. R.; Schlafer, N. J.; Janke, C. J.; Miller, E. A.; Thomas, M.; Addleman, R. S.; Bonheyo, G. T., Effect of Biofouling on the Performance of Amidoxime-Based Polymeric Uranium Adsorbents. Ind. Eng. Chem. Res. 2016, 55, (15), 4328-4338.

Appendix

A. Published Chemosphere article

The following provides the accepted Chemosphere manuscript of the first ToF-SIMS imaging and analysis of bilge emulsion.

Chemosphere 236 (2019) 124345

Contents lists available at ScienceDirect

Chemosphere

journal homepage: www.elsevier.com/locate/chemosphere

Short Communication

Surface evolution of synthetic bilgewater emulsion

Jiyoung Son [a], Yanjie Shen [a], Jenn Yao [a], Danielle Paynter [b], Xiao-Ying Yu [a, *]

[a] Energy and Environment Directorate, Pacific Northwest National Laboratory, Richland, WA, 99354, United States
[b] Naval Surface Warfare Center, Carderock Division, West Bethesda, MD, 20817, United States

HIGHLIGHTS

- Bilgewater surface change characterized by ToF-SIMS and optical microscopy.
- Aged emulsion droplets increase in size compared to fresh ones.
- Oil and detergent mix contribute to bilgewater in low mass organic components.
- Large organic components in detergent mix migrate to bilge over time.
- Some organics are consumed while new organics are formed during aging.

GRAPHICAL ABSTRACT

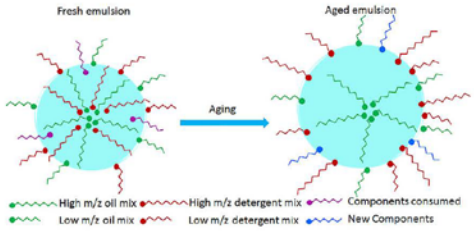

ARTICLE INFO

Article history:
Received 29 April 2019
Received in revised form
2 July 2019
Accepted 9 July 2019
Available online 16 July 2019

Handling Editor: Keith Maruya

Keywords:
Bilgewater
Droplet size distribution
ToF-SIMS
Surface composition
Surfactant
Oil-in-water

ABSTRACT

Bilgewater is a regulated shipboard produced waste stream that often contains oil-in-water emulsion. Fundamental knowledge of emulsion surface changes is required for improved wastewater treatment; however, limited information is currently available. We have reported the first surface characterization of synthetic bilgewater emulsions using time-of-flight secondary ion mass spectrometry (ToF-SIMS) coupled with optical microscopy. A Navy standard bilgewater solution consisting of a hydrocarbon and detergent mixture is used as the synthetic bilgewater emulsion model. Both fresh and aged emulsion samples are analyzed to determine their droplet size distributions (DSDs) and surface chemical composition. Our results show that fresh emulsions are largely mono-modal with hydrocarbon fragments as the main surface composition. Aged emulsions are also mono-modal with slightly larger size. Both SIMS spectral comparison and Principal Component Analysis (PCA) show that some surfactant components appear on the fresh emulsion surface while larger molecular weight components appear at the aged bilge droplet surface. Our results indicate that the oil-water interface evolves after emulsion droplet formation. More importantly, surface evolution not only changes the bilgewater DSD, but also alters the surface chemical composition and reactivity.

1. Introduction

Wastewater pollution has been a serious issue due to its widespread damage to the ocean. Among various potential ocean contaminants, bilgewater emulsions formed from various ship compartments has been an issue of concern (McLaughlin et al., 2014). The bilge of the vessel is the lowest space of the structure. Liquid wastes created through daily shipboard activities drain and are collected in a waste collection well. Typical bilgewater may contain water, oil, detergent, grease, solvents, chemicals, particles, and other materials (Ratledge, 1992) and is usually in a stable oil-in-

* Corresponding author.
E-mail address: xiaoying.yu@pnnl.gov (X.-Y. Yu).

https://doi.org/10.1016/j.chemosphere.2019.124345
0045-6535/

water (O/W) emulsion form. These oil droplets can range from a few micrometers to sub-micrometer in diameter. Due to their small diameters, bilgewater emulsions either require system residence times that are difficult to remove on shipboard or remain homogenous indefinitely. In addition, chemical bilgewater treatment is a non-viable option due to the constant variability of bilgewater influent (Chakrabarty et al., 2008). Because oil is entrained within bilgewater emulsions, a more sophisticated process than conventional skimming is required for emulsion breaking and oil removal, such as using dissolved air floatation or electrocoagulation. Thus development of methods and techniques to treat or to mitigate the formation and undesired consequences of shipboard emulsions (i.e., development of targeted treatment technologies or shipboard elimination of problematic surfactants) are urgently needed. In order to develop effective bilgewater treatment methods, it is important to understand the evolution at the oil and water liquid-liquid interface after bilgewater emulsions form.

There has been some recent efforts to understand O/W emulsion stability and chemical properties. Stabilized emulsions were recently investigated using two different surfactants to determine the effect of surfactant classification and salinity on emulsion formation and stability (Church et al., 2017). In another study, a stable O/W emulsion was characterized using sorbitan monooleate as the emulsifier, and it was found that the emulsion stability changed in correlation with emulsifier dosage, O/W ratio, stirring intensity, and temperature (Chen and Tao, 2005). These studies utilized surfactants and physical stirring tools (i.e., homogenizer, sonicator) to synthesize stable O/W emulsions.

To measure synthetic O/W emulsion stability, various characterization parameters, including contact angle, pH, oxidation reduction potential, and droplet size distribution need to be cross-evaluated. Increasingly, multiplexed characterization approaches are considered for in-depth understanding of emulsions (Chen and Tao, 2005; Church et al., 2017). However, emulsion droplet surface changes are non-obvious using bulk approaches.

Time-of-flight secondary ion mass spectrometry (ToF-SIMS) is a versatile surface analysis tool, and it can provide detailed elemental, molecular, and isotopic mapping of solid surfaces, thin films, or gas-solid interfaces. ToF-SIMS has been used in surface characterization in many applications such as biological cells, proteins, biofilms, corrosion, various materials (e.g., silicon wafer, polymers, and nanomaterials) and particles (Fu et al., 2018; Yu et al., 2018; Ding et al., 2019). In addition to spectral analysis, ToF-SIMS provides a two-dimensional (2D) and three-dimensional (3D) chemical mapping of surfaces (Sui et al., 2017). Although many types of surfaces have been characterized using ToF-SIMS, emulsions have not been widely studied using this approach (Davies et al., 1996).

Bilgewater is highly variable and can contain any percentage of portable water, seawater, and oils. As an initial study of bilge using advanced surface analysis, we will focus on the established NAVY synthetic bilge model (Church et al., 2017). Factors like salinity or pH will be pursued in the future. In this study, oil DSD changes between aged and fresh bilgewater emulsions were imaged using optical microscopy, and emulsion DSD was determined using an in-house droplet count Matlab software. The bilgewater surface changes between fresh and aged synthetic emulsions have been characterized by ToF-SIMS.

2. Material and methods

2.1. Bilgewater composition

The same procedure used in previous synthetic bilgewater generation studies have been adapted to study the emulsion surface changes in this work (Church et al., 2017). The synthetic emulsion sample consisted of a liquid mixture of 10 mL Navy Standard Bilge Mix (NSBM) #4 abbreviated as oil mix herein and 1 mL of detergent mix. The oil mix consists of 50% diesel fuel marine (MIL-PRF-16884 N), 25% 2190 TEP steam lube oil (MIL-PRF-17331K), and 25% 9250 diesel lube oil (MIL-PRF-9000L). The detergent mix consisted of 50% type 1 general purpose detergent (MIL-D-16791G (1)), 25% commercial detergent Tide Ultra (liquid), and 25% degreasing solvent (MIL-PRF-680C, Type III). The oil mix and detergent mix were provided by the collaborators at the Naval Surface Warfare Center, Carderock Division.

2.2. Optical microscopy and size determination

The DSD of the synthetic bilgewater emulsion was analyzed using an optical microscope (Nikon Eclipse TE2000-U). To obtain a clear individual oil droplet image, the emulsion sample was diluted with a ratio of 20 (deionized water, DI):1 (emulsion). Representative optical images of a fresh and 6-day aged emulsion sample are provided in Fig. 1. The DSS was determined using a Matlab program. More details are seen in supplementary information (SI).

2.3. ToF-SIMS surface analysis

A series of dry emulsion samples were prepared for ToF-SIMS analysis. Details of each sample are given in Table S1. A ToF-SIMS V instrument (IONTOF GmbH, Münster, Germany) was used. The pressure of the main chamber was maintained at ~1×10^{-8} mbar during analysis. The primary ion beam was a 25 keV Bi_3^+ with 10 kHz pulse energy. The pulse width was 0.8 ns and the current was ~0.6 pA. SIMS spectra were acquired by rastering over an area of $500 \times 500\ \mu m^2$ for 60 scans.

ToF-SIMS data was processed using the IONTOF Surface Lab 6.3 software. Calibrated spectra were exported to Origin Pro (2017) for plotting. Analysis reproducibility was verified (see Figs. S3 and S4). Spectral principal component analysis (PCA) was conducted using Matlab (version R2018a). Prior to conducting spectral PCA, SIMS spectral data were treated by mean-centering, normalization to the total ion intensity of selected peaks, square-root transformation (Sui et al., 2018). Additional experimental details are seen in SI.

3. Results and discussion

3.1. DSD of fresh and aged bilgewater

Fig. 1a &b depict a representative example of fresh and aged bilgewater droplets imaged using optical microscopy. The summary of optical microscopy DSD determination is provided in Table S2. Bilgewater emulsion droplet size seems to grow overtime. The average mean diameter of fresh bilge is 1.26 μm, and the aged is 1.38 μm. Both emulsions are monomodal. Coalescence seems to be a factor contributing to the size change from fresh bilge to aged bilge by comparing the optical images.

3.2. Bilgewater surface characterization

Fig. 2 depicts ToF-SIMS spectral comparison of fresh emulsion, aged emulsion, oil mix, detergent mix, and the Si substrate control (abbreviated as control herein) in the positive ion mode. Fig. S11 shows comparison of m/z^+ 500–800. Additional negative spectral comparisons are depicted in Figs. S10a–S10c.

Two trends are observed in Fig. 2. First, both oil mix and detergent mix contribute to the fresh and aged emulsion in the lower mass region (m/z^+ 1–250). Fresh and aged emulsions have hydrocarbon peaks, such as m/z^+ 41.038 $C_3H_5^+$, 55.054 $C_4H_7^+$, 57.071

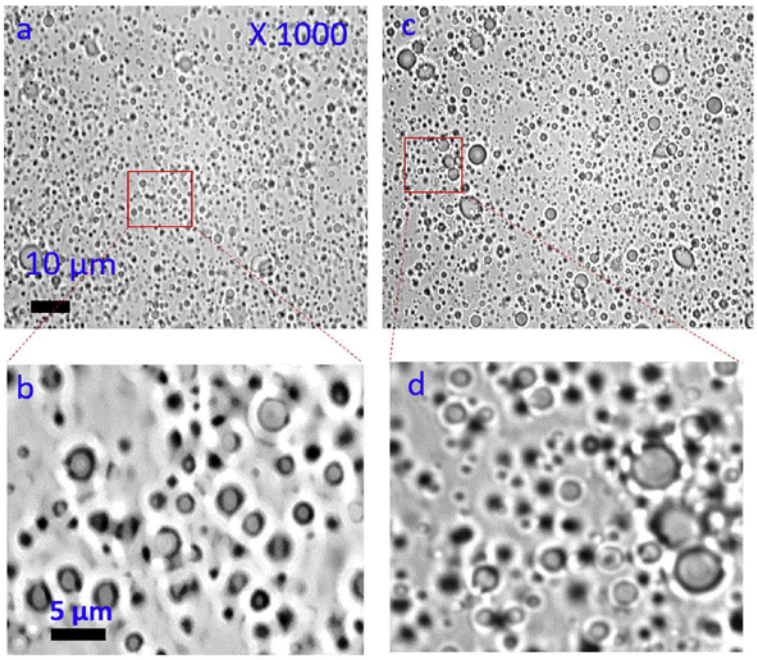

Fig. 1. Representative optical image of fresh (a, b) and aged (c, d) synthetic bilge emulsions.

$C_4H_9^+$, 71.088 $C_5H_{11}^+$, 91.047 $C_7H_7^+$, and 105.066 $C_8H_9^+$. Specifically, oil mix component peaks, such as m/z^+ 27.022 $C_2H_3^+$, 29.038 $C_2H_5^+$, 67.053 $C_5H_7^+$, 69.071 $C_5H_9^+$, 81.069 $C_6H_9^+$ (Li and Parnell, 2003) and detergent mix peaks (i.e., m/z^+ 22.990 Na^+, 45.033 $C_2H_5O^+$) contribute to the fresh and aged emulsion surface, suggesting that the oil and detergent components immediately appear at the surface of fresh bilge droplet and persist on the aged bilge droplet.

Second, pseudo-molecular ions $[M+H]^+$ peaks from the key components of detergents are observed and identified in the detergent mix, fresh bilge, and aged bilge emulsions in a wider m/z range (Figs. 2 and S11). For example, components of Triton m/z^+ 251.153 $C_{16}H_{27}O_2^+$ and polyethylene glycol m/z^+ 107.085 $C_4H_{11}O_3^+$. More detailed information is summarized in Table S3.

For the relatively higher masses (i.e., $m/z^+ > 500$), contribution from the oil mix to the emulsion surface is not as significant as the detergent mix. Distinct detergent peaks such as m/z^+ 507.276 $C_{22}H_{44}O_{11}Na^+$, 551.303 $C_{24}H_{48}O_{12}Na^+$, 595.323 $C_{26}H_{52}O_{13}Na^+$, 639.347 $C_{28}H_{56}O_{14}Na^+$, 683.370 $C_{30}H_{60}O_{15}Na^+$, 727.394 $C_{32}H_{64}O_{16}Na^+$, 771.417 $C_{34}H_{68}O_{17}Na^+$ are identified as fragments of D-tocopheryl polyethylene glycol succinate (TPGS, an efficient emulsifier) (Kong et al., 2011; Lu et al., 2013; Khare et al., 2016).

The intensity of these emulsifier peaks in aged emulsion is higher than that in fresh emulsion, indicating that the emulsion surface composition evolves over time. These dominant detergent peaks with larger molecular mass ($m/z^+ > 500$) provide direct evidence that surfactants with higher organic mass migrate into the surface after being inside the droplet initially. The SIMS spectral features suggest that the lower mass surfactant components (Figs. 2 and S11) necessitate emulsion formation, thus they appear on the fresh emulsion surface immediately. In contrast, relatively larger molecular weight components take longer to migrate to the droplet surface as observed in aged emulsions. In other words, 'aging' effect also changes chemical compositions of emulsion droplet surface besides changing the droplet size.

In addition, some species (i.e., m/z^+ 238.148, 334.334) only appear in fresh emulsion, and others only exist in the oil mix (e.g., m/z^+ 271.222 $C_{17}H_{35}O_2^+$). Such observation suggests that new organic species are formed on the emulsion surface as oil mix components are consumed and interacted with detergent mix and water over time. This is not surprising as secondary organics are known to form as a result of oxidation from primary organics such as hydrocarbons in ambient conditions (Waxman et al., 2013; Alpert et al., 2017). This finding indicates that reactions may take place at the emulsion surface, although these new components are not fully identified yet. Spectral comparisons in the negative ion mode (Figs. S10a–S10c) give similar observations and support the findings in the positive ion mode.

3.3. Surface evolution confirmed by PCA

All peak spectral PCA was conducted to confirm the spectral observation and identify additional features among emulsion samples and their components. PC1 explains 48.72% of data and mainly separates the Si substrate control and detergent mix from aged bilge, fresh bilge and oil mix. PC2 explains 30.92% of data and mainly separates the detergent mix from aged bilge, fresh bilge, and oil mix (Fig. S12a). PC3 as another important component explains 17.38% of data, and it separates oil mix and detergent mix from fresh and aged bilge. Comparing scores and loadings plots of the top five PCs, PC1, PC3, and PC4 give the most interesting results. Fig. 3a–e give the scores plots of PC1 vs PC3 and PC3 vs. PC4 as well as their loadings plots in the positive ion mode. Additional PCA results are shown in Figs. S12–S13.

Oil components are expected at the bilgewater emulsion surface. PC1 negative loadings share commonalities for oil mix, fresh, and aged bilge emulsions (Fig. 3a). This finding verifies that the oil

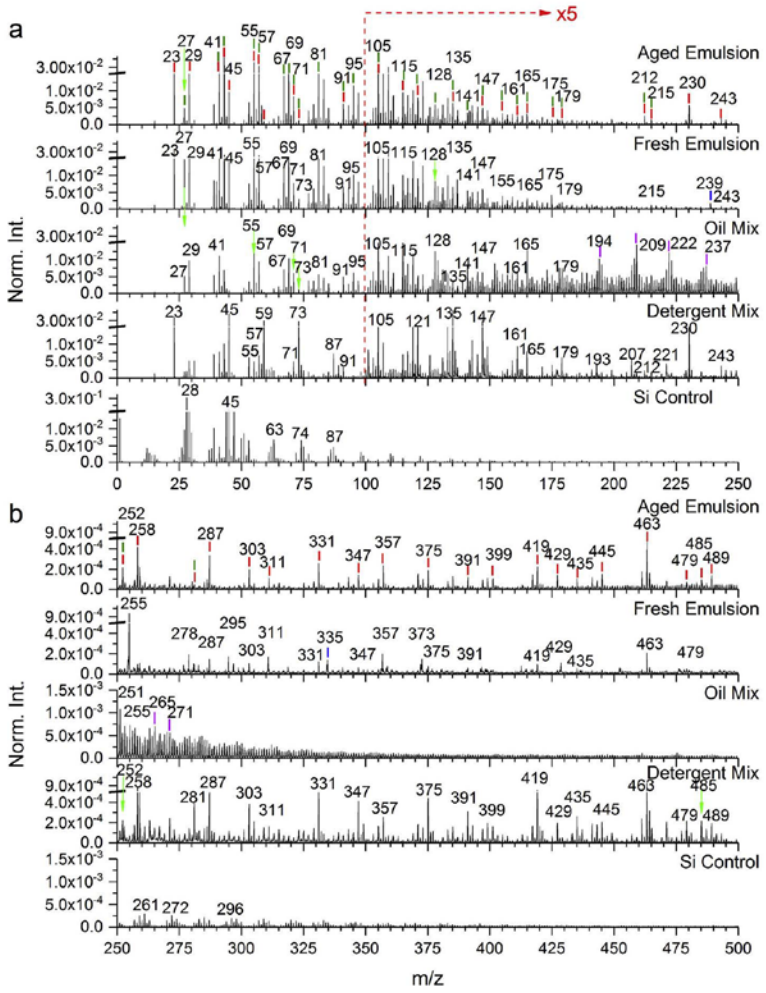

Fig. 2. ToF-SIMS spectral comparison of synthetic bilgewater emulsion and key components: (a) m/z^+ 0–250 and (b) 250–500 in the positive ion mode. The green, red, blue and purple lines represent oil, detergent, newly formed and consumed components, respectively. (For interpretation of the references to color in this figure legend, the reader is referred to the Web version of this article.)

mix is indeed an important component leading to the formation of bilgewater emulsion. Some characteristic peaks identified as components of the oil mix include hydrocarbon fragments such as m/z^+ 67 $C_5H_7^+$, 69 $C_5H_9^+$, 81 $C_6H_9^+$, and 119 $C_6H_{11}O_2^+$. In the relatively higher mass range (i.e., $200 < m/z^+ < 500$), some characteristic oil mix peaks are m/z^+ 227 $C_{13}H_{23}O_3^+$ and 271 $C_{17}H_{35}O_2^+$. PC1 positive separates the detergent mix from the oil mix, fresh bilge, and aged bilge emulsions. Similar to the oil mix, some characteristic detergent peaks appear immediately at the fresh emulsion surface, for example, TPGS fragments including m/z^+ 287 $C_{12}H_{24}O_6Na^+$, 331 $C_{14}H_{28}O_7Na^+$, 375 $C_{16}H_{32}O_8Na^+$, 419 $C_{18}H_{36}O_9Na^+$, and 435 $C_{18}H_{36}O_{10}Na^+$, 463 $C_{20}H_{40}O_{10}Na^+$, and 479 $C_{20}H_{40}O_{11}Na^+$. Most of them persist in the aged emulsion. Unlike the oil mix, the detergent mix components have more contribution to the fresh and aged emulsion in the higher mass organics, some examples are the TPGS fragments, such as m/z^+ 507, 551, 595, 639, 683, 727, and 771.

Fig. 3a depicts the PC3 vs. PC4 scores plot. The detergent mix has some components found in the oil mix. It is not surprising that oil mix and detergent mix components share some commonalities in PC3 negative. Peaks such as m/z^+ 23 Na^+, and 59 $C_3H_7O^+$ are representative of detergent components. Fresh and aged emulsions share commonalities in PC3 positive. Some representative peaks are m/z^+ 55 $C_4H_7^+$, 67 $C_5H_7^+$, 69 $C_5H_9^+$, 81 $C_6H_9^+$, and 107 $C_4H_{11}O_3^+$, which are hydrocarbon fragments as components of the oil mix (Li and Parnell, 2003). Other peaks contributing to this distinction are from the detergent mix including but not limited to TPGS emulsifier fragments as discussed earlier.

PC4 negative loadings in Fig. 3b and c shows distinct peaks of aged emulsion (e.g., m/z^+ 212, 230, 258, and 445), consistent with spectral comparison. Some peaks only exist in fresh emulsions as indicated in PC4 positive in Fig. 3c, for instance, m/z^+ 334. Many surfactant peaks appear both in aged and fresh emulsion surfaces, however, a few peaks only appear in the aged emulsion such as, m/z^+ 212, 230, 258, and 445, giving the evidence that new products

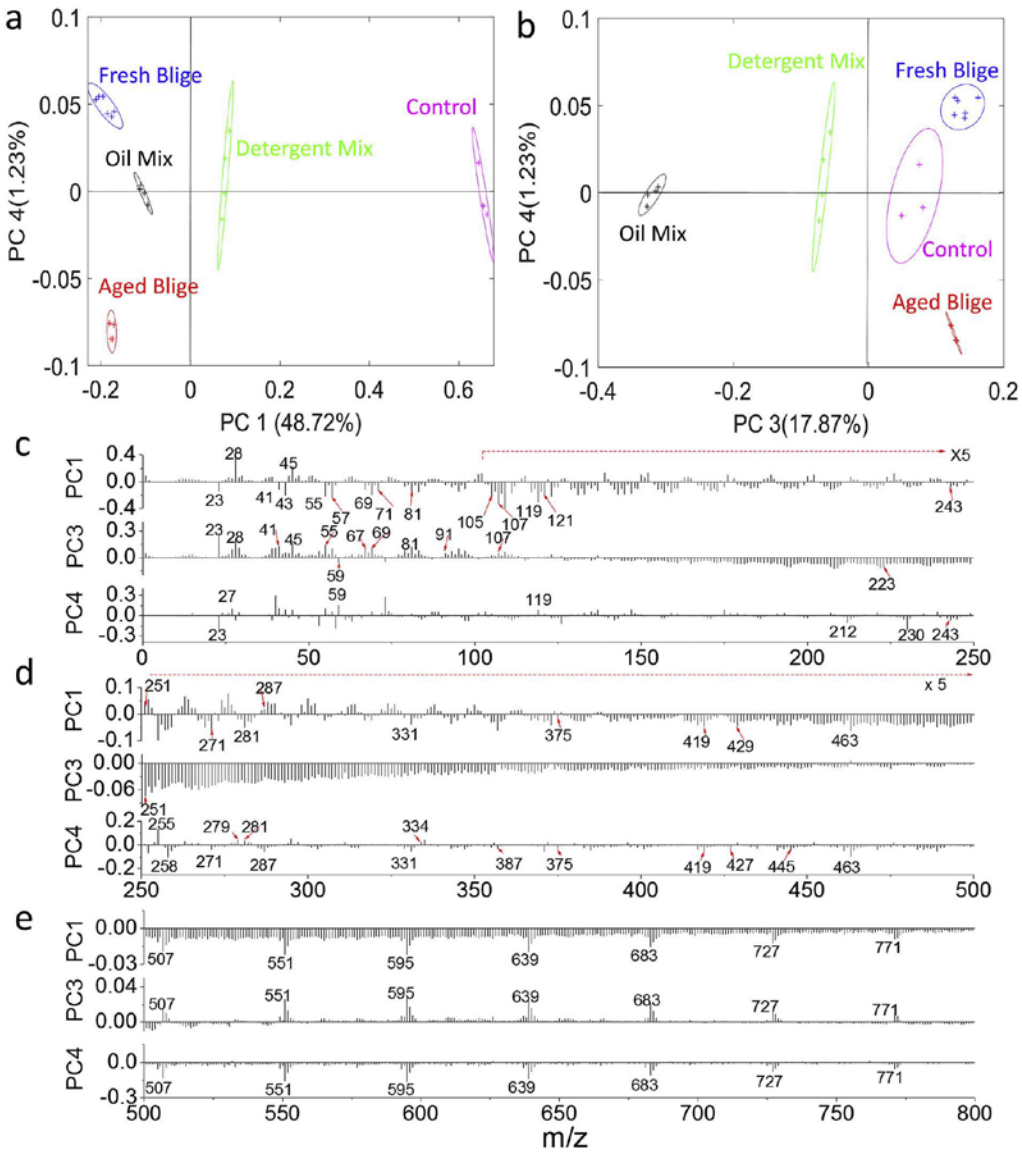

Fig. 3. Spectral PCA results of aged emulsion, fresh emulsion, oil mix, detergent mix, and Si control in the positive mode: Scores plots of PC1 vs. PC3 (a), PC4 vs. PC1 (b), PC1, PC3, and PC4 loadings plots in m/z^+ 0–250 (c), 250–500 (d), and 500–800 (e). Peaks are labelled in their center masses.

are formed during surface aging. Without the MS-MS SIMS capability (Fisher et al., 2016), it is difficult to unambiguously determine all the organic peaks at this time. Regardless, this finding shows the chemical surface change of O/W bilgewater droplets over time. Some surfactant peaks only appear in the fresh emulsion but not in the aged emulsion peaks. We postulate these peaks are consumed and form larger organic mass or secondary organics in the aged emulsion. This hypothesis requires verification with additional experiments using *in situ* liquid SIMS in the next step.

3.4. 2D bilgewater surface aging

Fig. 4 depicts the 2D comparison of selected key peaks observed in the fresh and aged bilge emulsion (Fig. 4a and b) in relation to the oil mix and detergent mix (Fig4. c and d) in the negative ion mode. The redder color indicates higher relative ion intensities and darker color lower intensities. The 2D image comparison results support the spectral observations in the positive ion mode. First, some component peaks of the oil mix and detergent mix are persistent in

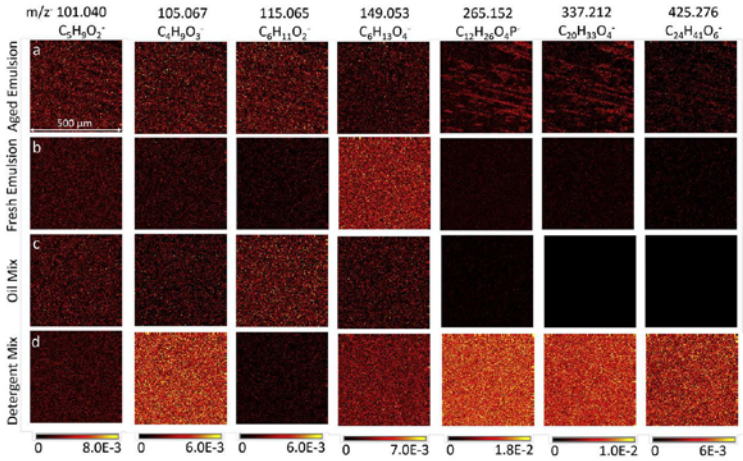

Fig. 4. Normalized 2D image comparison of key peaks in the negative mode: (a) aged emulsion sample, (b) fresh emulsion sample, (c) oil mix and (d) detergent mix sample. Normalization is done to the total ion intensities.

fresh and aged emulsions. Some examples include but not limited to the following, fatty acid m/z⁻ 101.040 $C_5H_9O_2^-$, 115.065 $C_6H_{11}O_2^-$ and polyethylene glycol (e.g., m/z⁻ 105.067 $C_4H_9O_3^-$, 149.053$C_6H_{13}O_4^-$). Second, surfactant components that are verified as the key components of the detergent mix seem to have higher contribution to the aged emulsion than fresh emulsion. For example, m/z⁻ 265.152 $C_{12}H_{26}O_4P^-$, 337.212 $C_{20}H_{33}O_4^-$, and 425.276 $C_{24}H_{41}O_6^-$ have higher relative intensities as the emulsion surface ages over time compared to the fresh one.

2D image comparisons of selected key peaks in the positive ion mode (Fig. S14) give similar observations and support the findings in the negative mode. Detailed information is in SI.

4. Conclusions

In conclusion, we have conducted the first surface characterization of synthetic bilgewater emulsions using a Navy model with coupled optical microscopy and ToF-SIMS. Our findings suggest that the aged emulsion not only grows in size but also has significant surface compositional changes. Both oil and detergent components appear in the emulsion surface as soon as fresh droplets form as expected. Higher mass organics from the surfactant components appear at the droplet surface as droplets age. Surface oxidation is another factor that modifies the emulsion chemical makeup over time, however, this effect is not significant. This is probably because the samples were prepared in a well-controlled nitrogen drying environment. Drying has an effect on the emulsion analysis results (Fu et al., 2018; Sui et al., 2018). One of the most significant effect is loss of the water phase. Although we can map oil and detergent components using the ToF-SIMS mass spectrometry imaging of dry emulsion samples, it is not possible to study the water phase in the O/W emulsion using static SIMS. Therefore, *in situ* liquid SIMS is planned to probe the dynamic oil-water liquid-liquid phase evolution in the near future.

Notes

The authors declare no competing financial interest.

CRediT authorship contribution statement

Jiyoung Son: Data curation, Formal analysis, Investigation, Methodology, Validation, Visualization, Writing - original draft, Writing - review & editing. **Yanjie Shen:** Formal analysis, Validation, Visualization, Writing - original draft, Writing - review & editing. **Jenn Yao:** Formal analysis, Software, Supervision, Writing - original draft. **Danielle Paynter:** Writing - original draft, Writing - review & editing. **Xiao-Ying Yu:** Conceptualization, Formal analysis, Funding acquisition, Investigation, Project administration, Resources, Software, Supervision, Validation, Writing - original draft, Writing - review & editing.

Acknowledgments

This work is performed under the support of the SERDP project WP18-1660. Pacific Northwest National Laboratory is operated by Battelle under Contract No. DE-AC05-76RL01830.

Appendix A. Supplementary data

Supplementary data to this article can be found online at https://doi.org/10.1016/j.chemosphere.2019.124345.

References

Alpert, P.A., Ciuraru, R., Rossignol, S., Passananti, M., Tinel, L., Perrier, S., Dupart, Y., Steimer, S.S., Ammann, M., Donaldson, D.J., George, C., 2017. Fatty acid surfactant photochemistry results in new particle formation. Sci. Rep. 7.
Chakrabarty, B., Ghoshal, A.K., Purkait, M.K., 2008. Ultrafiltration of stable oil-in-water emulsion by polysulfone membrane. J. Membr. Sci. 325, 427–437.
Chen, G., Tao, D., 2005. An experimental study of stability of oil–water emulsion. Fuel Process. Technol. 86, 499–508.
Church, J., Paynter, D.M., Lee, W.H., 2017. In situ characterization of oil-in-water emulsions stabilized by surfactant and salt using microsensors. Langmuir 33, 9731–9739.
Davies, M.C., Lynn, R.A.P., Hearn, J., Paul, A.J., Vickerman, J.C., Watts, J.F., 1996. Surface chemical characterization using XPS and ToF-SIMS of latex particles prepared by the emulsion copolymerization of methacrylic acid and styrene. Langmuir 12, 3866–3875.
Ding, Y., Zhou, Y., Yao, J., Xiong, Y., Zhu, Z., Yu, X.-Y., 2019. Molecular evidence of a toxic effect on a biofilm and its matrix. Analyst 144, 2498–2503.
Fisher, G.L., Bruinen, A.L., Ogrinc Potočnik, N., Hammond, J.S., Bryan, S.R., Larson, P.E., Heeren, R.M.A., 2016. A new method and mass spectrometer design for ToF-SIMS parallel imaging MS/MS. Anal. Chem. 88, 6433–6440.

Fu, Y., Zhang, Y., Zhang, F., Chen, J., Zhu, Z., Yu, X.-Y., 2018. Does interfacial photochemistry play a role in the photolysis of pyruvic acid in water? Atmos. Environ. 191, 36–45.
Khare, V., Sakarchi, W.A., Gupta, P.N., Curtis, A.D.M., Hoskins, C., 2016. Synthesis and characterization of TPGS–gemcitabine prodrug micelles for pancreatic cancer therapy. RSC Adv. 6, 60126–60137.
Kong, L.Y., Su, B.G., Bao, Z.B., Xing, H.B., Yang, Y.W., Ren, Q.L., 2011. Direct quantification of mono- and di-d-α-tocopherol polyethylene glycol 1000 succinate by high performance liquid chromatography. J. Chromatogr. A 1218, 8664–8671.
Li, R., Parnell, J., 2003. In situ microanalysis of petroleum fluid inclusions by Time-of-Flight-Secondary Ion Mass Spectrometry as an indicator of evolving oil chemistry: a pilot study in the Bohai Basin, China. J. Geochem. Explor. 78–79, 377–384.
Lu, J., Huang, Y., Zhao, W., Chen, Y., Li, J., Gao, X., Venkataramanan, R., Li, S., 2013. Design and characterization of PEG-derivatized Vitamin E as a nanomicellar formulation for delivery of paclitaxel. Mol. Pharm. 10, 2880–2890.
McLaughlin, C., Falatko, D., Danesi, R., Albert, R., 2014. Characterizing shipboard bilgewater effluent before and after treatment. Environ. Sci. Pollut. Res. 21, 5637–5652.
Ratledge, C., 1992. Biodegradation and biotransformations of oils and fats—introduction. J. Chem. Technol. Biotechnol. 55, 397–398.
Sui, X., Zhou, Y., Zhang, F., Chen, J., Zhu, Z., Yu, X.-Y., 2017. Deciphering the aqueous chemistry of glyoxal oxidation with hydrogen peroxide using molecular imaging. Phys. Chem. Chem. Phys. 19, 20357–20366.
Sui, X., Zhou, Y., Zhang, F., Zhang, Y., Chen, J., Zhu, Z., Yu, X.-Y., 2018. ToF-SIMS characterization of glyoxal surface oxidation products by hydrogen peroxide: a comparison between dry and liquid samples. Surf. Interface Anal. 50, 927–938.
Waxman, E.M., Dzepina, K., Ervens, B., Lee-Taylor, J., Aumont, B., Jimenez, J.L., Madronich, S., Volkamer, R., 2013. Secondary organic aerosol formation from semi- and intermediate-volatility organic compounds and glyoxal: relevance of O/C as a tracer for aqueous multiphase chemistry. Geophys. Res. Lett. 40, 978–982.
Yu, X.-Y., Yao, J., Lao, D.B., Heldebrant, D.J., Zhu, Z., Malhotra, D., Nguyen, M.-T., Glezakou, V.-A., Rousseau, R., 2018. Mesoscopic structure facilitates rapid CO_2 transport and reactivity in CO_2 capture solvents. J. Phys. Chem. Lett. 9, 5765–5771.

B. Published PCCP front cover and hot article

The following provides the published PCCP manuscript of the first in situ SEM and in situ ToF-SIMS imaging and analysis of the NAVY bilge emulsion. This article was also selected to be in the 2020 Hot Article issue by the editors of PCCP for its high quality.

Volume 22
Number 21
7 June 2020
Pages 11749–12324

PCCP

Physical Chemistry Chemical Physics

rsc.li/pccp

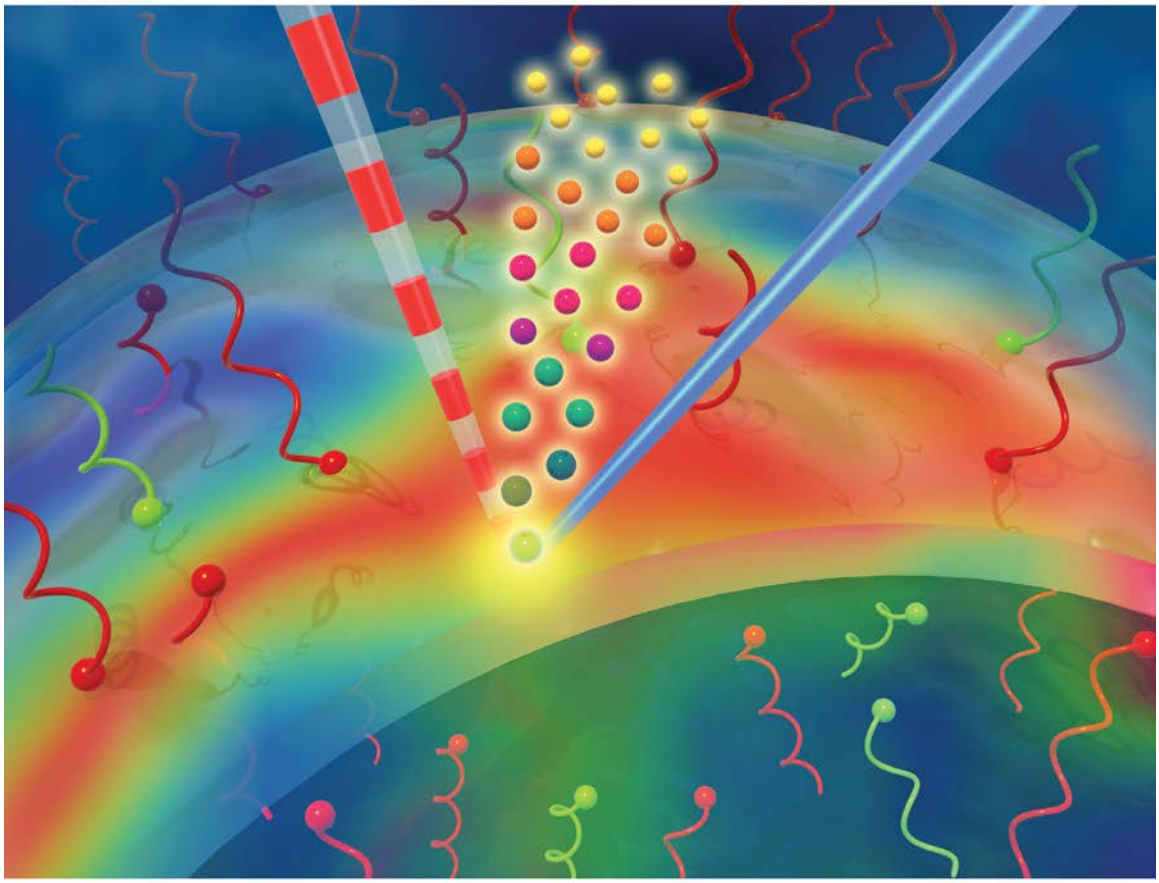

ISSN 1463-9076

ROYAL SOCIETY OF CHEMISTRY

PAPER
Xiao-Ying Yu *et al.*
Liquid ToF-SIMS revealing the oil, water, and surfactant interface evolution

PCCP

PAPER

Cite this: *Phys. Chem. Chem. Phys.*, 2020, **22**, 11771

Liquid ToF-SIMS revealing the oil, water, and surfactant interface evolution†

Yanjie Shen, [a] Jenn Yao, ‡[a] Jiyoung Son, ‡[a] Zihua Zhu [b] and Xiao-Ying Yu *[a]

Bilge water from ships is regarded as a major pollutant in the marine environment. Bilge water exists in a stable oil-in-water (O/W) emulsion form. However, little is known about the O/W liquid–liquid (l–l) interface. Traditional bulk characterization approaches are not capable of capturing the chemical changes at the O/W l–l interface. Although surfactants are deemed essential in droplet formation, their roles in bilge water stabilization have not been fully revealed. We have utilized novel *in situ* chemical imaging tools including *in situ* scanning electron microscopy (SEM) and *in situ* time-of-flight secondary ion mass spectrometry (ToF-SIMS) to study the evolving O/W interface using a NAVY bilge model for the first time. The droplet size distribution (DSD) does not change significantly without the addition of X-100 surfactants under static or rocking conditions. Both the oil components and the water clusters are shown to evolve over time at the O/W droplet interface by *in situ* liquid SIMS imaging. Of particular interest to droplet stabilization, the contribution of surfactants to the aged bilge droplets becomes more significant as the droplet size increases. The higher mass surfactant component does not appear on the droplet surface immediately while many lower mass surfactants are solvated inside the droplet. We have provided the first three-dimensional images of the evolving O/W interface and demonstrated that *in situ* surface chemical mapping is powerful enough to reveal the complex and dynamic l–l interface in the liquid state. Our observational insights suggest that surfactants are important in mediating droplet growth and facilitating effective separation of bilge water emulsion.

Received 31st January 2020,
Accepted 29th February 2020

DOI: 10.1039/d0cp00528b

rsc.li/pccp

Introduction

Due to rapid development of sea transportation, pollution in the marine environment has caught attention worldwide. Bilge water, a wastewater mainly formed from ships, is regarded as a major pollutant to the marine environment.[1–3] Typically, bilge water is a mixture of seawater, oily fluids, detergent fluids, lubricants, particles, and other similar wastes; and it usually exists in a stable oil-in-water (O/W) emulsion form.[4–7] It contains hazardous substances and can cause damage to the water quality and endanger the environment. Moreover, it is toxic to aquatic biological systems as well as human health. Several chemical and physical methods have been developed to treat bilge water, such as flotation, separation by centrifugation, filtration, and coagulation.[8] However, the treatment of bilge emulsion in the presence of oil, detergent, and particles is difficult using physical methods, especially when the diameter of the emulsified oil droplet is below 20 μm.[9] Known methods of bilge water treatment are not efficient universally, including ultrafiltration, wet air oxidation, electrocoagulation, the use of biotechnology, and membrane distillation.[8,10–13] Thus, new methods to treat bilge water are urgently needed. To facilitate method development, it is important to understand the properties of bilge water emulsion, including the formation, stability, breaking, and evolution of emulsion droplets at the O/W liquid–liquid (l–l) interface under conditions relevant to onboard ships.[14,15]

A few recent papers reported experimental studies of O/W emulsion stability. Optical microscopy including confocal laser scanning microscopy, atomic force microscopy, and scanning electron microscopy (SEM) were used to characterize O/W emulsions.[16–19] Salinity and pH were shown to be associated with emulsion breaking and separation processes.[14,20] The emulsifier dosage, ratio of oil to water, stirring intensity, emulsifying temperature, and mixing time also have an effect on droplet stability using conventional measurements.[21–24] However, the evolution of chemical changes at the O/W l–l interface cannot be characterized using known bulk approaches.

[a] *Energy and Environment Directorate, Pacific Northwest National Laboratory, Richland, WA 99354, USA. E-mail: xiaoying.yu@pnnl.gov*
[b] *Environmental Molecular Sciences Laboratory, Pacific Northwest National Laboratory, Richland, WA 99354, USA*

† Electronic supplementary information (ESI) available: Additional experimental details and results. See DOI: 10.1039/d0cp00528b

‡ Equal contribution.

Our group developed a novel vacuum compatible microreactor, or System for Analysis at the Liquid Vacuum Interface (SALVI), enabling multimodal imaging of liquids using vacuum instruments.[25–27] *In situ* liquid time-of-flight secondary ion mass spectrometry (ToF-SIMS) has proven to be a powerful tool to study liquid surfaces, air–liquid (a–l), l–l, and solid–liquid interfaces. It provides detailed elemental, molecular, and isotopic mapping of the surface or interface in biology, materials, and the environment. ToF-SIMS itself provides more than one mode of measurement, offering spectral, two-dimensional (2D), and three-dimensional (3D) chemical mapping of surfaces and interfaces.[28–30]

To further the emulsion interfacial research using *in situ* imaging and based on our recent dry SIMS surface characterization, we propose the following hypotheses of the evolution of the O/W interface in bilge water emulsion: (1) water plays a critical role in the O/W interface; (2) low mass oil and detergent components (*i.e.*, m/z^+ 0–250) and relative high mass surfactant components (*i.e.*, m/z^+ 250–500) appear immediately in the fresh bilge water surface and persist in the aged bilge water; (3) high mass surfactant components (*i.e.*, m/z^+ 500–800) may take time to migrate to the surface; and (4) surface surfactant composition has an effect on the emulsion DSD. This work is the first *in situ* chemical imaging study of emulsion using new chemical imaging tools including *in situ* scanning electron microscopy (SEM) and *in situ* ToF-SIMS. *In situ* liquid SEM has been first used to determine the change in droplet size distribution (DSD) of oil droplets between fresh and aged bilge water emulsions. *In situ* liquid SIMS has been used to study the evolution of O/W emulsions at the l–l interface as the surface ages and given visualization of the surfactant, oil components, and water in the liquid state. Optical microscopy was used to quickly assess the effect of surfactants on the DSD evolution of bilge water with and without X-100 enhancement over the course of six days.

Experimental

Emulsion sample preparation

Components of the oil mix and detergent mix were provided by our collaborator at the Naval Surface Warfare Center, Carderock Division; and they were used to generate synthetic bilge emulsion. The synthetic emulsion consists of a liquid mixture of 10 mL oil mix (Navy Standard Bilge Mix (NSBM) #4) and 1 mL detergent mix. The detailed procedure has been reported previously.[14] Briefly, the oil mix contains 50% diesel fuel marine (MIL-PRF-16884N), 25% 2190 TEP steam lube oil (MIL-PRF-17331K), and 25% 9250 diesel lube oil (MIL-PRF-9000L). The detergent mix contains 50% type 1 general purpose detergent (MIL-D-16791G (1)), 25% commercial detergent Tide Ultra (liquid), and 25% degreasing solvent (MIL-PRF-680C, type III).[15] Fresh bilge refers to emulsions prepared following the reported procedure and immediately followed by *in situ* analysis without sitting or rocking. Aged bilge refers to emulsions analyzed 24 h after preparation. To study the effect of surfactants, a bilge sample was prepared with extra X-100 surfactants compared to the NAVY recipe. This sample is referred to as X100 + fresh bilge. More details of all the liquid emulsion samples are given in Table S1 (ESI†).

The prepared bilge liquids are injected into the SALVI microchannel prior to *in situ* SEM and *in situ* liquid ToF-SIMS chemical imaging. Optical microscopy was also used to obtain images for DSD determination. To obtain clear images of individual oil droplets, the emulsion sample was diluted using deionized (DI) water before *in situ* SEM imaging and optical imaging. As a comparison, dried droplets were analysed using static ToF-SIMS to offer better mass accuracy. Additional experimental details of static ToF-SIMS sample preparation were presented previously[15] and in the ESI.†

SALVI device fabrication

The details of SALVI device fabrication were described in our previous publications.[31,32] In general, the SALVI device consists of a polydimethylsiloxane (PDMS) block with a 200 μm (width) × 300 μm (depth) microfluidic channel inside, a 100 nm thick silicon nitride (SiN) membrane (Norcada, Canada) with a window of 1.5 × 1.5 mm^2 on a supporting silicon frame (7.5 × 7.5 mm^2). In addition, PTFE tubing is used to introduce a liquid to the microfluidic channel. Fig. 1c and d show the schematic of SALVI coupled with *in situ* liquid SEM and *in situ* liquid SIMS, respectively.

In situ liquid SEM

The SiN membrane detection window of the SALVI device was coated with 10 nm thick carbon prior to *in situ* SEM imaging to reduce the charging effect. The microfluidic device was injected with approximately 100 μL liquid sample (*e.g.*, bilge water emulsion) and sealed with a PEEK union. The loaded SALVI device was mounted on the SEM stage and stabilized with double-sided copper tape to further reduce charging. More details were reported previously.[33,34] The backscattered electron (BSE) images were acquired in the high vacuum mode. The vacuum in the chamber was maintained at $\sim 4 \times 10^{-6}$ Torr. The accelerating voltage and current were set at 20 kV and 0.11 nA, respectively.

The SEM images of the bilge droplets were pre-processed using ImageJ to enhance the contrast. The image analysis of the DSDs of fresh and aged emulsions was done by fitting the data with a lognormal distribution model in MATLAB (MathWorks, MATLAB 2018b). The lognormal model is often used as a default model for regression analysis of particle size.[35] Table S2 (ESI†) provides fitting results of the DSD obtained from *in situ* SEM.

Optical microscopy

Optical microscopy (Nikon Eclipse TE2000-U) was used to study the effect of surfactant on the droplet size growth in bilge water emulsion with and without X-100 over six days under both static and rocking conditions. In static conditions, the emulsion mixture was allowed to sit in the hood for six days and an aliquot was taken from the mixture for DSD determination daily. No additional sonication was used before analysis.

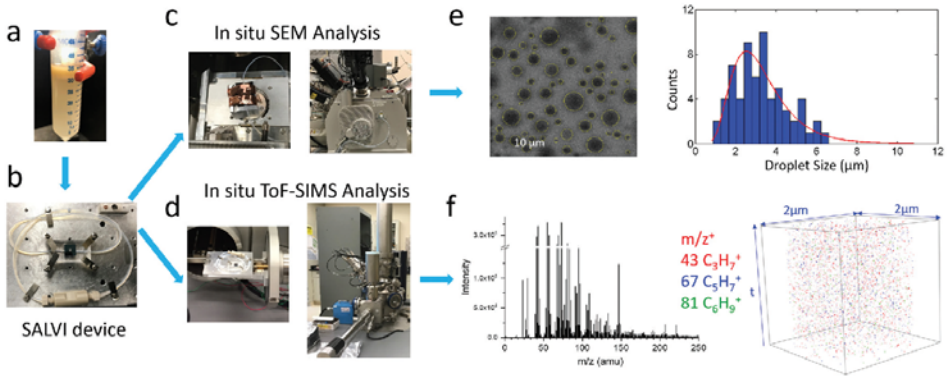

Fig. 1 The schematic showing bilge water and liquid sample preparation for multimodal imaging analysis: (a) liquid bilge water emulsions after mechanical mixing and sonication; (b) a SALVI device filled with emulsion; (c) *in situ* liquid SEM measurements of bilge water; (d) *in situ* liquid ToF-SIMS analysis of bilge water; (e) DSD determination using *in situ* SEM; and (f) a representative ToF-SIMS mass spectrum and 3D image.

During rocking, the emulsion mixture was stationed in a platform shaker (INNOVA 2300, New Brunswick Co., Inc.) to shake at 180 rpm continuously for six days and DSD determination was determined daily. All samples were analysed using 1000 times of magnification and droplet images were collected using a digital CCD camera (Hamamatsu, C4742-95-12HR) on an inverted microscope (Nikon Eclips TE2000-U). The pixel size information was processed and given by the MetaMorph® software with a resolution of ~92 nm. The camera captured images at 4000 (H) by 2624 (V) pixels. At least six images were acquired for each sample. A Matlab program was used to determine the DSD (Table S3, ESI†).

ToF-SIMS

A ToF-SIMS V instrument (IONTOF GmbH, Münster, Germany) was used for *in situ* liquid SIMS. During liquid ToF-SIMS, the SiN membrane was punched through using a pulsed Bi_3^+ ion beam (25 KeV, 10 kHz, pulse width 150 ns). As the primary ion beam made a hole of 2 μm in diameter on the SiN membrane, the SIMS image of the liquid surface was collected for 100 s for 2D and 3D image analysis. Then the Bi_3^+ ion beam continuously sputtered on the liquid surface for 200 s with a reduced pulse width of 80 ns to acquire spectral measurements. Before each analysis, the 1 KeV O_2^+ beam was used to clean the SiN membrane with a scanning area of 200 μm × 200 μm to remove surface contamination from the atmosphere. At least 4 data points were acquired for each sample in the positive and negative ion mode, respectively. The main chamber pressure was maintained around 4×10^{-7} mbar during analysis. The analysis depth of liquid ToF-SIMS is approximately less than 10 nm.[31,36,37] Fig. S3 and S4 (ESI†) show the reproducibility of the liquid ToF-SIMS mass spectra. During static ToF-SIMS analysis of dried emulsion samples, a standard procedure was followed.[15]

The ToF-SIMS mass spectral data was processed using IONTOF Surface Lab 6.3 software. The mass spectra were calibrated using OH (*m/z* 17), SiC_2H_5O (*m/z* 73), $Si_2C_3H_9O_3$ (*m/z* 149), and $Si_3C_5H_{15}O_4$ (*m/z* 223) in the negative mode; and CH_3^+ (m/z^+ 15), $(CH_3)_3Si^+$ (m/z^+ 73), $Si_2OC_5H_{15}^+$ (m/z^+ 147), $Si_3C_5H_{15}O_3^+$ (m/z^+ 207), and $Si_4O_4C_7H_{21}^+$ (m/z^+ 281) in the positive mode, respectively. Spectral principal component analysis (PCA) was conducted using MATLAB software.

In the first round of PCA, the known interference peaks were removed, for example, *m/z* 1 H , 12 CH , 16 O , 24 C_2 , 25 C_2H , 28 Si , 29 SiH , 41 SiCH , $SiCH_2$, 44 SiO , 45 SiOH , 58 $SiCH_2O$, 59 $SiCH_3O$,60 SiO_2 , 73 SiC_2H_5O , 75 $SiCH_3O_2$, 149 $Si_2C_3H_9O_3$, 163 $Si_2C_5H_{15}O_2$, 223 $Si_{13}C_9H_{15}O_4$, and 237 $Si_3C_7H_{21}O_3$ in the negative mode; and m/z^+ 28 Si^+, 59 CH_3SiO^+, 73 $(CH_3)_3Si^+$, 147 $Si_2O_5H_{15}^+$, 207 $Si_3C_5H_{15}O_3^+$, 281 $Si_4O_4C_7H_{21}^+$, 369 $Si_5O_4C_{11}H_{33}^+$, 209 Bi^+, 418 Bi_2^+, and 657 Bi_3^+ in the positive mode. In the second round of PCA, peaks were selected using the following criteria: (1) the intensity of the peak in the ToF-SIMS mass spectrum was significantly higher than its neighboring peaks (*i.e.*, S/N > 3); (2) product peaks were identified using reference spectra of dry samples in the static SIMS analysis;[15] (3) known water cluster peaks; and (4) the peaks in the SIMS mass spectrum with m/z^+ or *m/z* > 40. The mass calibrated data were treated by normalization to the total selected ion intensity, square-root transformation, and mean entering before running spectral PCA.[25,38]

Results and discussions

In situ SEM determination of DSD

Fig. 2 depicts the representative SEM BSE images of the fresh and aged bilge droplets. Fig. S1a and S1b (ESI†) show more SEM results. Both fresh and aged bilge have mainly monomodal size distribution. Table S2 (ESI†) gives the summary of the DSD determination using *in situ* liquid SEM. The measurements illustrate that bilge emulsion droplets change slightly in

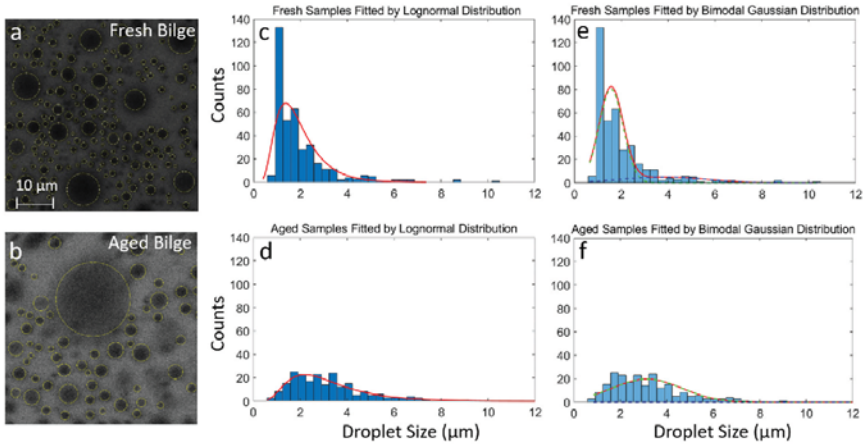

Fig. 2 Representative *in situ* liquid SEM images (a and b) and histograms showing fresh and aged bilge DSD determination using the lognormal (c and d) and bimodal Gaussian distribution (e and f), respectively.

size over time. The SEM images show that the droplet increases from the mean diameter of 1.69 ± 0.43 μm in the fresh bilge to 3.12 ± 0.26 μm in the aged one after one day using the bimodal fitting. When using the lognormal distribution to analyze DSD, the results are slightly different, *i.e.*, 1.98 ± 0.55 μm and 3.35 ± 1.06 μm for fresh and aged bilge emulsion, respectively. The results using bimodal and lognormal fittings are slightly different, however, showing a similar trend. This finding confirms that the droplet does not remain the same once formed and changes over time.

Coagulation does occur even in fresh bilge emulsion. A bimodal Gaussian distribution fit was conducted combining all valid *in situ* SEM images (Fig. 2). The observations show that only a small percentage of bilge droplets quickly coalesce. The bimodal fitting results suggest that the majorities of drops are in the primary mode, *i.e.*, 1.57 ± 0.51 μm and 3.15 ± 1.49 μm for fresh and one-day aged bilge emulsion (abbreviated as aged hereafter). The secondary mode is 3.81 ± 1.79 μm for fresh and 25.33 ± 1.61 μm for aged bilge emulsion. Thus, the lognormal fit is reasonable to explain most data. Larger droplets are easier to handle in bilge water separation. Fresh and aged bilge water emulsions tend to be less than 4 μm, thus not so easy to treat. We focus on the *in situ* surface chemical analysis of the primary mode or the smaller droplets with a diameter of one to several micrometers in this work.

Bilge water DSD evolution

Optical microscopy was used to quickly assess DSD evolution of bilge water with and without X-100 addition over the course of six days at static and gently rocking conditions (Fig. S2a and b, ESI†). In static conditions, DSD increased from 1.29 ± 0.51 μm from the freshly prepared bilge to 1.87 ± 1.03 μm for that on day 6 without the addition of X-100 (Fig. S2a, ESI†). When adding X-100, coagulation was immediately significant. The DSD in the latter case ranged from 4.66 ± 4.72 μm from the freshly prepared emulsion sample to 17.54 ± 50.64 μm on day 6. The X-100 surfactant seems to have a more significant effect on the emulsion DSD growth compared to just time alone. The large variance of DSDs in the X-100 enhanced bilge water sample shows that extremely large droplets frequently form under static conditions. This observation suggests that the X-100 surfactant can promote coagulation of droplets to a large size randomly as time elapses.

In contrast, when gently rocking the bilge water samples with and without X-100 surfactants, the results are different. The DSD does not change significantly for bilge water as expected (Fig S2b, ESI†), because shaking helps prevent coagulation and mimics the gentle collisions encountered in flowing water. However, when adding X-100 surfactant to the bilge water, the DSD under rocking conditions shows a growth pattern in six days despite a slight delay compared to that in static conditions. The droplets grow from 5.17 ± 5.76 μm to 19.01 ± 15.60 μm. This finding supports the hypothesis that surfactants like X-100 have a significant effect on the emulsion DSD growth mainly by mediating the surface chemistry. In addition, coagulation is significant in rocking conditions, like in static conditions. In contrast, the DSD grows much larger when adding extra X-100 surfactant to the bilge water, further illustrating the effect of surface chemistry on DSD change. More information on DSD is summarized in Table S3 (ESI†). In the following, we focus on the effect of surfactants on the evolved O/W interfacial chemistry.

In situ ToF-SIMS imaging of the O/W interface

Looking into the positive ion mass comparison plots (Fig. 3 and Fig. S5, ESI†), oil components are observed in the fresh bilge, aged bilge, and X-100 + fresh bilge in the low mass range

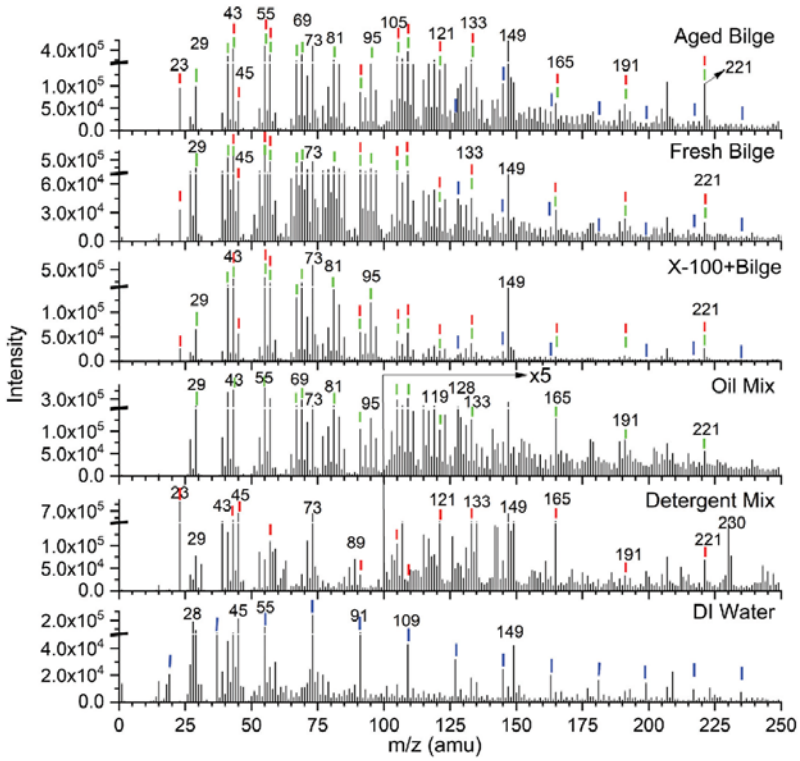

Fig. 3 *In situ* liquid ToF-SIMS spectral comparison of synthetic bilge water emulsions and key components in m/z^+ 0–250. Green, red, and blue bars represent oil, detergent, and water cluster peaks, respectively.

(*i.e.*, m/z^+ 1–250). Most of the characteristic peaks are identified as hydrocarbon fragments, such as m/z^+ 41 $C_3H_5^+$, 57 $C_4H_9^+$, 67 $C_5H_7^+$, 69 $C_5H_9^+$, 71 $C_5H_{11}^+$, 81 $C_6H_9^+$, 91 $C_7H_7^+$, 105 $C_8H_9^+$, and 121 $C_9H_{13}^+$. In the higher mass range (*i.e.*, m/z^+ 250–500), only a small fraction of high mass peaks from the oil mix are observed in the fresh bilge, aged bilge, and X100 + fresh bilge samples. In the high mass range (*i.e.*, m/z^+ 500–800), no significant oil peaks are observed in the bilge samples. We previously studied dried bilge samples using static ToF-SIMS and hypothesized that the bilge surface would evolve over time.[15] However, water is lost in dry sample analysis. In this work using liquid SIMS, our results provide a more direct evidence that oil components mainly contribute to the peaks in the low mass range. They appear immediately in the fresh bilge surface and persist in the aged bilge. Lower mass peaks of the detergent components have a similar behavior. In contrast, higher mass detergent components show different behaviors.

Spectral composition between static and *in situ* ToF-SIMS

High mass resolution analysis using dry samples was performed to provide confident reference spectra for peak identification in liquid ToF-SIMS. The details of dry sample preparation, static ToF-SIMS analysis, and peak identification were reported recently.[15] Comparisons of the peaks in static dry samples and dynamic liquid samples show that the mass to charge (m/z) ratios are in good agreement. Thus, peak identification using unit mass in liquid SIMS is reasonable, and it is based on reference spectral analysis in static ToF-SIMS with a higher mass accuracy. The key peak identification is presented in Table 1 and more information is shown in Tables S4 and S5 (ESI†).

Oil and detergent components in bilge water

Fig. 3 and Fig. S5 (ESI†) depict the liquid SIMS spectral comparison of the fresh bilge, aged bilge, X-100 + fresh bilge, oil mix, detergent mix, and DI water in the positive ion mode. Detergent mix and oil mix share some common peaks in the low mass range (*i.e.*, m/z^+ 1–250); and most of them are identified as hydrocarbon peaks, such as m/z^+ 41 $C_3H_5^+$, 57 $C_4H_9^+$, 71 $C_5H_{11}^+$, 91 $C_7H_7^+$, 105 $C_8H_9^+$, and 121 $C_9H_{13}^+$. Several high peaks are observed in the detergent mix in the relative high mass range (m/z^+ 250–500), such as m/z^+ 331, 347,

Table 1 Key possible peak identification in the positive and negative mode

m/z^+_{exact}	$m/z^+_{obs.}$	Formula	Chemical description	Ref.
41.039	41	$C_3H_5^+$	Hydrocarbon	39
43.055	43	$C_3H_7^+$	Hydrocarbon	39
55.055	55	$C_4H_7^+$	Hydrocarbon	39
57.070	57	$C_4H_9^+$	Hydrocarbon	39
67.055	67	$C_5H_7^+$	Hydrocarbon	39
69.070	69	$C_5H_9^+$	Hydrocarbon	39
71.086	71	$C_5H_{11}^+$	Hydrocarbon	39
81.070	81	$C_6H_9^+$	Hydrocarbon	39
91.055	91	$C_7H_7^+$	Hydrocarbon	39
105.070	105	$C_8H_9^+$	Hydrocarbon	39
121.102	121	$C_9H_{13}^+$	Hydrocarbon	39
243.121	243	$C_{10}H_{20}O_6Na^+$	Fragment of TPGS	15
507.278	507	$C_{22}H_{44}O_{11}Na^+$	Fragment of TPGS	40
551.304	551	$C_{24}H_{48}O_{12}Na^+$	Fragment of TPGS	40
595.330	595	$C_{26}H_{52}O_{13}Na^+$	Fragment of TPGS	40
639.356	639	$C_{28}H_{56}O_{14}Na^+$	Fragment of TPGS	40
683.382	683	$C_{30}H_{60}O_{15}Na^+$	Fragment of TPGS	40
m/z^-_{exact}	$m/z^-_{obs.}$	Formula	Chemical description	Ref.
49.008	49	C_4H^-	Hydrocarbon	*a*
63.023	63	$C_5H_3^-$	Hydrocarbon	*a*
79.055	79	$C_6H_7^-$	Hydrocarbon	*a*
105.055	105	$C_4H_9O_3^-$	Polyethylene glycol	*b*
205.217	205	$C_{12}H_{29}O_2^-$	Polyethylene glycol	*b*
221.081	221	$C_{12}H_{13}O_4^-$	Diethyl phthalate	*b*
255.232	255	$C_{16}H_{31}O_2^-$	*n*-Hexadecanoic acid	*b*
325.063	325	$C_{18}H_{14}O_4P^-$	Triphenyl phosphate	*b*
337.238	337	$C_{20}H_{33}O_4^-$	Triton X-41	*b*
425.290	425	$C_{24}H_{41}O_6^-$	Triton X-45	*b*
513.343	513	$C_{28}H_{49}O_8^-$	Triton X-114	*b*

[a] Based on the molecular weight. [b] Reference is from the PubChem database.[41]

419, and 463. However, they are not observed in the fresh bilge, aged bilge, or X-100 + fresh bilge sample analysis using *in situ* liquid SIMS. This finding indicates that the contribution from detergent components is not as significant in the relative high mass range. This result is different from dry emulsion analysis. In dry samples, these detergent peaks were observed in bilge water emulsions, especially in the aged emulsion.[15]

This discrepancy prompts a postulation that the surface chemistry is different from what was conceived based on dry emulsion surface analysis previously. In addition, it gives the observational evidence that dry emulsion does not fully represent the liquid droplet environment. One disadvantage of dry sample analysis is the loss of water in the O/W interface. Consequently, dry samples cannot offer direct observations of the changing O/W interface in liquid. In contrast, liquid SIMS makes up the traditional SIMS deficiency and gives 2D and 3D images of the dynamic l–l interface. In the O/W liquid environment, some peaks from the detergent mix in the m/z^+ 250–500 range disappear in the aged bilge surface in liquid; however, they are observed in dry samples. This interesting finding suggests that these detergent components may prefer to be solvated in liquid and remain in the bulk liquid inside the droplet. This may lead to the impression that the components on the bilge droplet surface are mainly small hydrocarbon chemicals from oil mixtures and surfactants. When the liquid sample becomes dry, these solvated components could appear in the bilge surface due to loss of water.

Observations are different in the high mass range, *i.e.*, m/z^+ 500–800. Unlike the oil components that have negligible contributions to the bilge surface composition, the detergent components are the main contributors. Significant detergent peaks are fragments of D-tocopheryl polyethylene glycol succinate (TPGS), an efficient emulsifier,[15,42–44] including m/z^+ 507 $C_{22}H_{44}O_{11}Na^+$, 551 $C_{24}H_{48}O_{12}Na^+$, 595 $C_{26}H_{52}O_{13}Na^+$, 639 $C_{28}H_{56}O_{14}Na^+$, and 683 $C_{30}H_{60}O_{15}Na^+$. These detergent peaks have dominant appearance in the aged bilge surface; however, they are not observed in the fresh emulsion at all. This finding suggests that these large molecular weight components do not appear immediately in the fresh bilge surface. In addition, these surfactant peaks migrate to the droplet surface over time. This result is similar to what was found in dry bilge samples. The observation of large surfactant peaks in the liquid bilge surface confirms that large molecular weight components take longer to move to the droplet surface, which is postulated based on dry droplet surface analysis. Additionally, the observation of these high molecular weight surfactants in both static and liquid ToF-SIMS may suggest that these surfactants are not situated as deep in the droplet bulk liquid phase, perhaps they exist in the thin film of the l–l interface as the bilge water emulsion forms initially. This may explain why they could be more easily observed in both the static and liquid ToF-SIMS unlike some of the mid-mass range detergent components. The latter may be located deeper in the bulk of the droplet. Molecular dynamic simulations would be helpful to elucidate and verify this postulation in the future.

Water cluster in bilge water

Water clusters are observed in the detergent mix and play a crucial role in forming bilge droplets. Water clusters marked by blue bars in Fig. 3 and Fig. S5 (ESI†) are spread in the detergent mix and bilge samples in a wide mass range. In the lower mass range of m/z^+ 1–250, the characteristic water clusters are $(H_2O)_nH^+$, n = 7, 8, 10, 11, 12, or 13. In the relative high mass range (*i.e.*, m/z+ 250–500), representative water clusters are featured as the following $(H_2O)_nH^+$, n = 14–20. The low intensity of water clusters indicates that these water clusters are not the main composition in the bilge surface. It also confirms that some detergent components (*e.g.*, m/z^+ 250–500) dissolved in liquid hardly move to the bilge surface. In the high mass range (*i.e.*, m/z^+ 500–800), no obvious water clusters are observed at the bilge surface. This may also be attributed to the much lower ion yields of larger water clusters. The existence of water clusters makes the bilge surface different over time when comparing fresh and aged droplets in liquid, and this is probably due to hydrogen bonding and other types of weak intermolecular interactions. Additionally, water cluster distribution varies over time, contributing to the different bilge surface composition. The negative spectral comparison in Fig. S6 (ESI†) shows similar results to those in the positive mode. More information is provided in the ESI.†

The l–l interface change confirmed by spectral PCA

To better understand the bilge water surface compositional changes between emulsion samples and their components,

selected peak spectral PCA is conducted in the positive and negative mode, respectively. In the negative mode, principal components (*e.g.*, PC1, PC2 and PC3) explain 92.15% of all data. PC1 explains 42.91% of data and mainly separates the DI water control, oil mix, and fresh bilge from aged bilge and detergent mix. It is not surprising that the X-100 + fresh bilge sample crosses over PC1 positive and negative, because it consists of emulsions and an extra amount of X-100. The latter is a popular detergent component and surfactant. PC2 explains 32.25% of data and mainly separates the detergent mix and DI water from the aged bilge, fresh bilge, oil mix, and detergent mix. PC3 explains 16.99% of all data and mainly separates the fresh bilge and detergent mix from the aged emulsion and DI water (Fig. 4).

In PC1 negative mode loadings, oil mix, fresh bilge and water cluster are the main contributors. Oil mix peaks, such as m/z 49 C_4H^-, 63 $C_5H_3^-$, 79 $C_6H_7^-$ and water clusters, such as m/z $(H_2O)_nOH^-$, n = 2, 3, 5, 6, 9, and 10, make contributions to the formation of fresh bilge. PC1 positive separates aged bilge and detergent mix from fresh bilge and oil mix. This finding suggests that the bilge surface composition changes over time, and that detergent components contribute more to the aged emulsion. Some detergent peaks, especially in the relative high mass range, identified as m/z 325 $C_{18}H_{14}O_4P^-$ and 337 $C_{20}H_{33}O_4^-$, only exist in the aged bilge but not fresh bilge. This indicates that these detergent components do not appear immediately in the fresh bilge surface yet move to the aged bilge surface as time elapses. This finding confirms the earlier hypothesis that the chemical surface composition change in O/W bilge water droplets over time using *in situ* molecular imaging.

The PC2 positive scores show that oil mix, fresh bilge, aged bilge and X-100 + fresh bilge share the same peaks. This finding suggests that some oil components, such as m/z 49 C_4H^-, 63 $C_5H_3^-$, and 79 $C_6H_7^-$, and detergent components, such as m/z 105 $C_8H_9^-$, 205 $C_{12}H_{29}O_2^-$ and 221 $C_{12}H_{13}O_4^-$, appear immediately in the fresh bilge and persist in the aged bilge over time. The PC2 negative scores show that the detergent mix shares common peaks with DI water. This makes sense because the detergent mix contains water. In PC3 positive, oil and detergent components have similar peaks, and both contribute to fresh bilge and X100 + fresh bilge. Characteristic peaks include m/z 49 C_4H^-, 205 $C_{12}H_{29}O_2^-$, 425 $C_{24}H_{41}O_6^-$ and 513 $C_{28}H_{49}O_8^-$. PC3 negative separates aged bilge and DI water from fresh bilge and detergent mix, which further confirms that the bilge surface composition changes over time. In addition, water clusters, such as m/z $(H_2O)_nOH^-$, n = 3–6 and 9–10, make contributions to the aged bilge. The X-100 + fresh bilge sample shares common peaks with fresh and aged bilge as anticipated. Overall, the observation of water clusters in both fresh and aged bilge indicates that water clusters play a vital role in the formation of bilge emulsion. Our results demonstrate that the bilge surface composition changes over time. Detergent components, especially those appearing in the aged but not fresh bilge, are in the high mass range, further confirming the change of bilge surface as a result of surface evolution from surfactants. The change in water cluster distributions and diffusion may also play a central role in this surface change. Further research would require theoretical simulation to investigate this phenomenon and provide more fundamental insights.

The scores plots of PC1 *vs.* PC2, PC1 *vs.* PC3, and their loading plots in the positive mode are presented in Fig. S7 (ESI†). These plots in the positive mode show agreement with those in the negative mode. Detailed information is provided in the ESI.†

3D imaging of the evolved O/W interface

3D images are very useful in visualizing the spatial distribution of chemical species.[30] Normalized 3D images of selected key peaks are used to study the evolution of chemical species at the O/W l–l interface in this work. Fig. 5 shows reconstructed and normalized 3D images in the positive mode; the color brightness indicates the relative intensity of a particular peak. The hydrocarbon fragments (*e.g.*, m/z^+ 43 $C_3H_7^+$, 67 $C_5H_7^+$, and 81 $C_6H_9^+$) appear in fresh and fresh + X-100 bilge. The hydrocarbon peaks have good abundance in the aged bilge, supporting the finding that the hydrocarbon components appear in the fresh bilge immediately and persist in the aged bilge over time.

The detergent components are evenly distributed in the detergent mix, for example, m/z^+ 243 $C_{10}H_{20}O_5Na^+$, 551 $C_{24}H_{48}O_{12}Na^+$, and 595 $C_{26}H_{52}O_{13}Na^+$. However, they do not contribute significantly in the fresh bilge, especially in the large mass range (*i.e.*, m/z^+ 551, 595). In the aged bilge, these larger detergent components have higher relative abundance and thus they are more dominant contributors to the surface chemical makeup. The contrast of detergent components in the fresh and aged bilge indicates that the existence of these large surfactant species is not noticeable immediately on the surface of the fresh bilge droplets. Instead, they migrate to the bilge droplet surface over time. Our results further confirm that the O/W interface evolves chemically in surface composition and physically in size.

Water clusters including but not limited to m/z^+ 199 $(H_2O)_{11}H^+$, 235 $(H_2O)_{13}H^+$, and 325 $(H_2O)_{18}H^+$ are well distributed in the detergent mix, fresh, and aged bilge water emulsions. In the detergent mix, a higher abundance of $(H_2O)_{11}H^+$ is seen. In comparison, the relative abundances of $(H_2O)_{13}H^+$ and $(H_2O)_{18}H^+$ are higher in the fresh and aged bilge water. This finding indicates that the water cluster distribution changes and affects the surface water hydrogen bonding environment.

Reconstructed 3D images of selected key peaks in the negative mode in Fig. 5b show similar findings. The hydrocarbon fragments, such as m/z 49 C_4H^-, 63 $C_5H_3^-$, and 79 $C_6H_7^-$, appear in the fresh bilge and fresh + X-100 bilge emulsions. As the droplet surface ages, the hydrocarbon components become evenly distributed in space. This observation supports the hypothesis that the hydrocarbon components appear in the fresh bilge immediately and persist in the aged bilge over time. The detergent components are homogeneously distributed in the detergent mix, for example, m/z 105 $C_{14}H_9O_3^-$, 221 $C_{12}H_{13}O_4^-$, and 255 $C_{16}H_{31}O_2^-$. They also are evenly distributed in the fresh bilge, aged bilge, and X-100 + fresh bilge emulsions. When looking

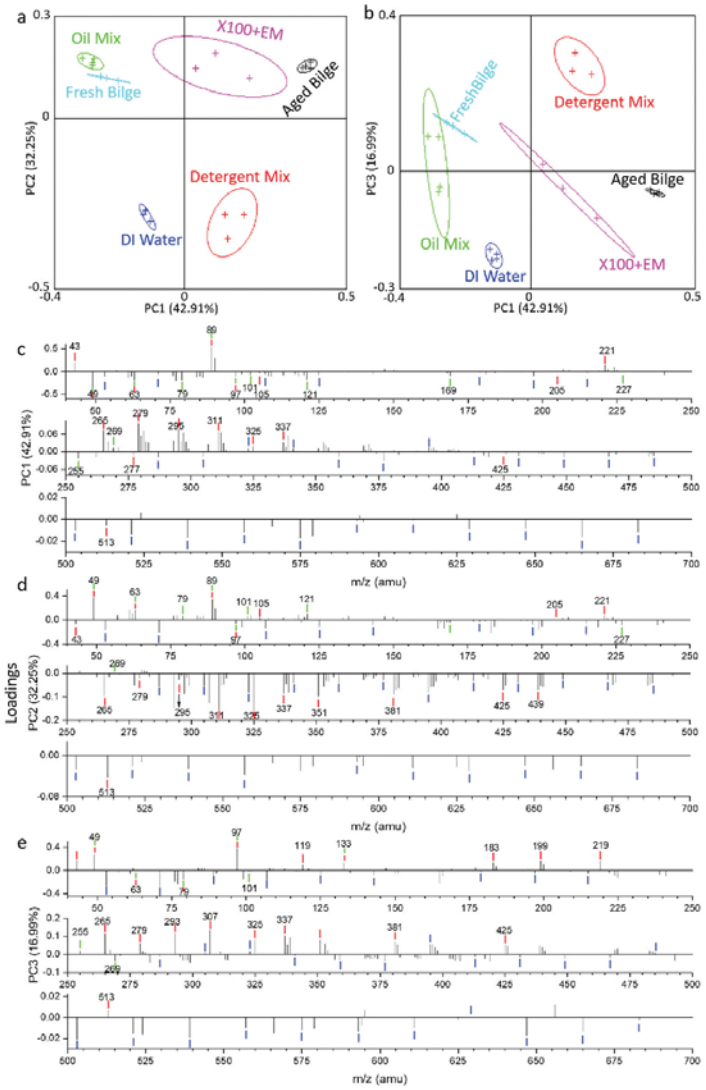

Fig. 4 Selected peak spectral PCA results in the negative mode: (a) Scores plots of PC1 *vs.* PC2; (b) scores plots of PC1 *vs.* PC3; and loadings plots of PC1 (c), PC2 (d), and PC3 (e), respectively. Peaks are labeled in their unit masses.

into the relative intensity of the same detergent peaks between the fresh bilge and aged bilge, the relative percentages of these components change over time. For example, *m/z* 221 $C_{12}H_{13}O_4$ has a higher relative intensity in the aged bilge. This finding also supports the hypothesis that the l–l interface has evolved over time. Water clusters are observed in all samples except the oil mix, and they are key components of both fresh bilge and aged bilge emulsions. This observation verifies that water is an essential liquid phase at the O/W interface in emulsion formation.[41]

New insight into the O/W interface

To better understand the evolution of the O/W interface, we further compare the results obtained in static ToF-SIMS and dynamic liquid ToF-SIMS. Static SIMS (Fig. 3 and Fig. S5, ESI†) gives the analysis of dry samples (Fig. S8, ESI†) and the results were published previously.[15] Liquid SIMS probes the l–l interface and gives direct visualization of the liquid environment.[27,33] Fig. 6 is a schematic illustration based on the liquid ToF-SIMS results. As a surface technique, the analysis depth of ToF-SIMS is known to be the top few nm of a material. When using ice as an approximation, liquid ToF-SIMS is probing the top layer of the oil–water interface approximately less than 10 nm (Fig. 6b and d).[31,36,37] It is worth noting that the data spots in the 3D images do not represent a fixed location of the ion due to liquid diffusion,[31] and they offer a representation of the chemical species spatial distribution of the thin layer of liquid being probed by the primary ion beam. Because of the diffusion of liquid, only the top layer of the liquids can be imaged using *in situ* liquid ToF-SIMS. At the vacuum–liquid interface, the temperature drop was estimated to be ~12 K if starting the experiment at room temperature. This temperature change will not induce freezing and has a slight effect on the diffusion rate of ions. The concentration change was estimated to be approximately 1.2–2.2 times of the initial concentration.[31] In addition, the diffusion rates of oil and the O/W mixture are different. In the original design of SALVI, we considered the self-diffusion constants of small ions and water to be in the range of 1–3 × 10^{-5} cm^2 s^{-1}.[31,45] The diffusion constants of oils are much slower than water[46] and the temperature dependence study of oils showed an insignificant effect on the diffusion constants.[47] The dynamic viscosity of single droplets of diesel emulsions does not vary much with high water to diesel ratios.[48]

The SIMS spectral comparison indicates that the liquid ToF-SIMS can reveal the l–l interface compared to static SIMS. The lower mass oil fragments and detergent components (*e.g.*, m/z^+ 0–250) migrate to the l–l interface immediately and persist in aged bilge water as time goes, as evidenced by liquid ToF-SIMS spectral observations. The relative high mass detergent components (*e.g.*, m/z^+ 250–500) are more likely to exist in the bulk liquid in a droplet underneath the surface, because SIMS imaging could not detect them in either fresh or aged droplet surfaces in the liquid state (Fig. S5a, ESI†). Interestingly, the high mass detergent components (*e.g.*, m/z^+ 507 $C_{22}H_{44}O_{11}Na^+$,

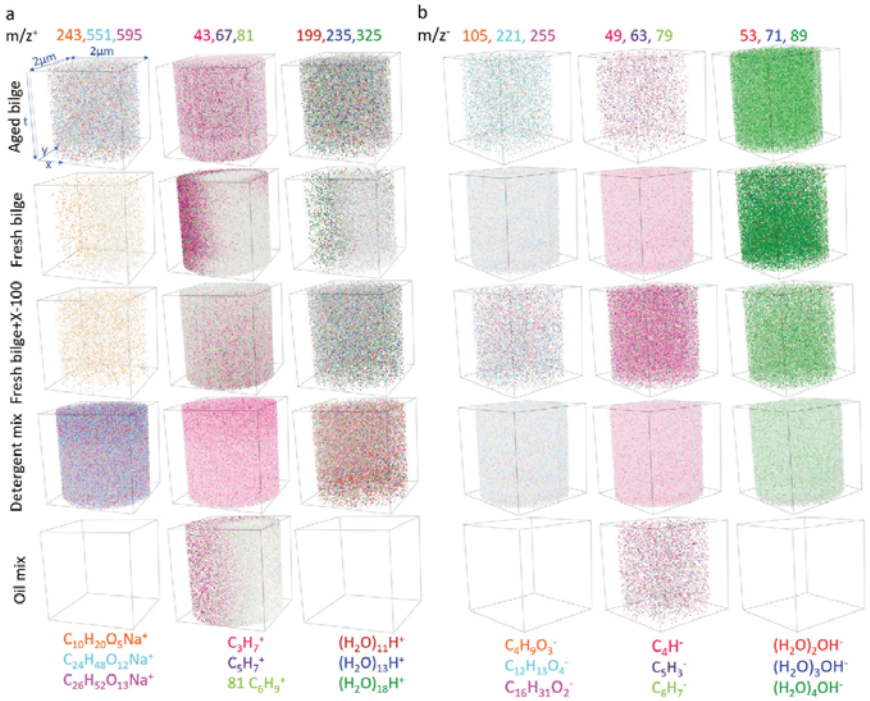

Fig. 5 Comparison of normalized 3D images of key peaks in the positive (a) and negative mode (b). Darker colors indicate higher relative peak intensities and light colors indicate lower intensities.

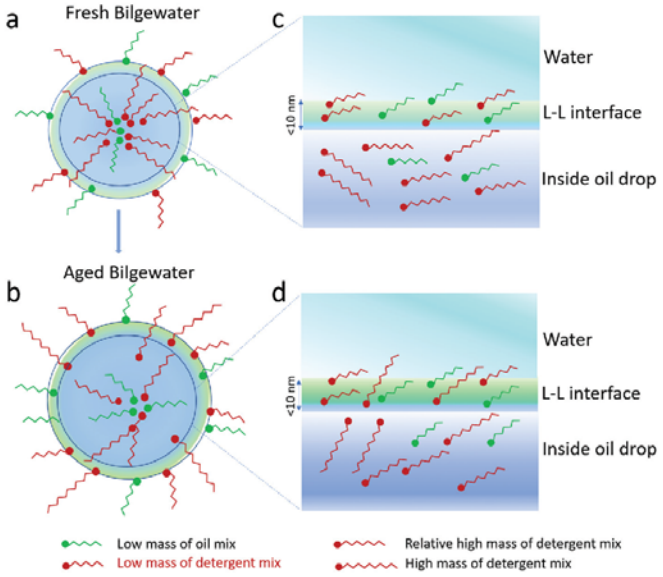

Fig. 6 The schematic showing the evolution of the O/W interface in fresh bilge water (a and c) and aged bilge water (b and d), respectively. (a and c) Depict a single droplet; (b and d) the interfacial region of a bilge water emulsion droplet.

551 $C_{24}H_{48}O_{12}Na^+$, 595 $C_{26}H_{52}O_{13}Na^+$, 639 $C_{28}H_{56}O_{14}Na^+$, and 683 $C_{30}H_{60}O_{15}Na^+$} may exist closer to the top of the liquid, however, likely below the 10 nm of the l–l interface initially. These surfactant components move to the top of the l–l interface after one day and get detected by *in situ* liquid ToF-SIMS (Fig. 6c and d). Although the static analysis of dry samples gives similar results concerning the low and high mass surfactant peaks, it misses the solvated mid-range mass fragments due to drying and water loss by collapsing the liquid structure (Fig. S8b, ESI†). Thus, *in situ* liquid ToF-SIMS provides a unique tool to observe the l–l interfacial change and gives us new insight into the evolution of the O/W interface, which was previously not possible.

Conclusions

We investigated the O/W l–l interface characterization of synthetic bilge water emulsions based on a Navy model using *in situ* SEM, optical microscopy, and *in situ* liquid SIMS. We found that the bilge water DSD is largely monodisperse; however, infrequent coagulation occurs even in freshly prepared bilge emulsions. The mean droplet size changes slightly as time elapses for bilge water without X-100 at static or gentle rocking conditions. However, the DSD becomes much larger for the bilge water with additional X-100 under either static or rocking conditions. This finding indicates time itself is insufficient to promote droplet growth and that the addition of surfactants like X-100 has a stronger influence on the DSD. Furthermore, the O/W l–l interfacial chemical composition evolves over time. We verified some of the hypotheses based on static dry emulsion results obtained in this work. First, our new finding suggests that water clusters play a crucial role in the formation and evolution of bilge water emulsion. Second, both oil and small detergent components appear in the O/W interface as soon as fresh droplets form as expected. Although high mass organics from the surfactant components do not appear immediately at the l–l interface, they migrate to the droplet surface as time passes. Our liquid SIMS observations reveal that some organic components in the mid-mass range (*i.e.*, *m*/*z* 250–500) are more likely to remain solvated and stay in the bulk of the liquid phase inside the droplet, therefore, they do not appear on the droplet surface. Such an observation is illuminating to further the surface chemistry of droplet composition and understand the evolving O/W interface.

In situ liquid SIMS offers us a unique chance to visualize the water phase in the O/W emulsion compared to static SIMS. The latter loses the information of water due to emulsion drying. In this work, we have first demonstrated that the bilge water emulsion interface involving water, oil, and surfactants in the liquid phase can be studied using novel *in situ* multimodal imaging. More systematic studies of factors, such as salinity, pH, surfactants, that affect bilge water emulsion stabilization and weakening using this Navy model would be interesting for

future work. Equally important is the theoretical modeling of the dynamic l–l interface that affects the chemistry of the droplet.

Conflicts of interest

The authors declare no competing financial interest.

Acknowledgements

This work was performed under the support of the SERDP project WP18-1660. The EMSL user proposals 50569 and 51176 were used for instrument access. We thank Danielle Paynter of NAVY CARDROCK for providing the NAVY bilge water model. We thank Michael Perkins of Pacific Northwest National Laboratory (PNNL) for graphic support. We thank William Chrisler for access to the optical microscopy at PNNL. PNNL is operated by Battelle under Contract No. DE-AC05-76RL01830. The processed data is available to readers by sending a request to the corresponding author, Dr Xiao-Ying Yu (xiaoying.yu@pnnl.gov).

References

1 J. Ge, J. Zhang, F. Wang, Z. Li, J. Yu and B. Ding, *J. Mater. Chem. A*, 2017, **5**, 497–502.
2 Z. Wang, X. Jiang, X. Cheng, C. H. Lau and L. Shao, *ACS Appl. Mater. Interfaces*, 2015, **7**, 9534–9545.
3 Y. Zhu, J. Wang, F. Zhang, S. Gao, A. Wang, W. Fang and J. Jin, *Adv. Funct. Mater.*, 2018, **28**, 1804121.
4 P. A. Alpert, R. Ciuraru, S. Rossignol, M. Passananti, L. Tinel, S. Perrier, Y. Dupart, S. S. Steimer, M. Ammann, D. J. Donaldson and C. George, *Sci. Rep.*, 2017, **7**, 12693.
5 J. Church, J. G. Lundin, D. Diaz, D. Mercado, M. R. Willner, W. H. Lee and D. M. Paynter, *Sci. Total Environ*, 2019, **691**, 981–995.
6 A. A. Umar, I. B. M. Saaid, A. A. Sulaimon and R. B. M. Pilus, *J. Pet. Sci. Eng.*, 2018, **165**, 673–690.
7 J. P. Chaudhary, N. Vadodariya, S. K. Nataraj and R. Meena, *ACS Appl. Mater. Interfaces*, 2015, **7**, 24957–24962.
8 K. Ulucan and U. Kurt, *J. Electroanal. Chem.*, 2015, **747**, 104–111.
9 J. A. Caplan, C. Newton and D. Kelemen, *Mar. Technol.*, 2000, **37**, 111–115.
10 B. K. Körbahti and K. Artut, *Desalination*, 2010, **258**, 219–228.
11 C. Akarsu, Y. Ozay, N. Dizge, H. Elif Gulsen, H. Ates, B. Gozmen and M. Turabik, *Water Sci. Technol.*, 2016, **74**, 564–579.
12 X. Mei, H. Wang, D. Hou, F. L. Lobo, D. Xing and Z. J. Ren, *Front. Environ. Sci. Eng.*, 2019, **13**, 53.
13 S. Putatunda, S. Bhattacharya, D. Sen and C. Bhattacharjee, *Int. J. Environ. Sci. Technol.*, 2018, **16**, 2525–2536.
14 J. Church, D. M. Paynter and W. H. Lee, *Langmuir*, 2017, **33**, 9731–9739.
15 J. Son, Y. Shen, J. Yao, D. Paynter and X.-Y. Yu, *Chemosphere*, 2019, **236**, 124345.
16 M. Ding, T. Zhang, H. Zhang, N. Tao, X. Wang and J. Zhong, *Food Hydrocolloids*, 2019, **95**, 326–335.
17 M. Ding, T. Zhang, H. Zhang, N. Tao, X. Wang and J. Zhong, *Food Chem.*, 2020, **309**, 125642.
18 T. Zhang, M. Ding, N. Tao, X. Wang and J. Zhong, *LWT*, 2020, **117**, 108654.
19 T. Zhang, M. Ding, H. Zhang, N. Tao, X. Wang and J. Zhong, *Food Chem.*, 2020, **308**, 125597.
20 H. Eskandarloo, M. J. Selig and A. Abbaspourrad, *Chem. Eng. J.*, 2018, **335**, 434–442.
21 G. Chen and D. Tao, *Fuel Process. Technol.*, 2005, **86**, 499–508.
22 K. Abdolmaleki, M. A. Mohammadifar, R. Mohammadi, G. Fadavi and N. M. Meybodi, *Carbohydr. Polym.*, 2016, **140**, 342–348.
23 C. W. Angle, T. Dabros and H. A. Hamza, *Chem. Eng. Sci.*, 2006, **61**, 7309–7324.
24 I. Vyrides, E. M. Drakou, S. Ioannou, F. Michael, G. Gatidou and A. S. Stasinakis, *J. Environ. Manage.*, 2018, **217**, 356–362.
25 Y. Ding, Y. Zhou, J. Yao, Y. Xiong, Z. Zhu and X.-Y. Yu, *Analyst*, 2019, **144**, 2498–2503.
26 Y. Fu, Y. Zhang, F. Zhang, J. Chen, Z. Zhu and X.-Y. Yu, *Atmos. Environ.*, 2018, **191**, 36–45.
27 X.-Y. Yu, J. Yao, D. B. Lao, D. J. Heldebrant, Z. Zhu, D. Malhotra, M.-T. Nguyen, V.-A. Glezakou and R. Rousseau, *J. Phys. Chem. Lett.*, 2018, **9**, 5765–5771.
28 X. Sui, Y. Zhou, F. Zhang, J. Chen, Z. Zhu and X.-Y. Yu, *Phys. Chem. Chem. Phys.*, 2017, **19**, 20357–20366.
29 F. Zhang, X. Yu, J. Chen, Z. Zhu and X.-Y. Yu, *npj Clim. Atmos. Sci.*, 2019, **2**, 28.
30 F. Zhang, X. Yu, X. Sui, J. Chen, Z. Zhu and X.-Y. Yu, *Environ. Sci. Technol.*, 2019, **53**, 10236–10245.
31 L. Yang, X.-Y. Yu, Z. H. Zhu, T. Thevuthasan and J. P. Cowin, *J. Vac. Sci. Technol., A*, 2011, **29**, 061101.
32 L. Yang, X.-Y. Yu, Z. Zhu, M. J. Iedema and J. P. Cowin, *Lab Chip*, 2011, **11**, 2481–2484.
33 J. Yao, D. B. Lao, X. Sui, Y. Zhou, S. K. Nune, X. Ma, T. P. Troy, M. Ahmed, Z. Zhu, D. J. Heldebrant and X.-Y. Yu, *Phys. Chem. Chem. Phys.*, 2017, **19**, 22627–22632.
34 X.-Y. Yu, B. Arey, S. Chatterjee and J. Chun, *Surf. Interface Anal.*, 2019, **51**, 1325–1331.
35 X. Yang, J. Lee, D. E. Barker, X. Wang and Y. Zhang, *J. Air Waste Manage. Assoc.*, 2012, **62**, 725–735.
36 A. M. Piwowar, S. Keskin, M. O. Delgado, K. Shen, J. J. Hue, I. Lanekoff, A. G. Ewing and N. Winograd, *Surf. Interface Anal.*, 2013, **45**, 302–304.
37 C. Szakal, J. Kozole, M. F. Russo, Jr., B. J. Garrison and N. Winograd, *Phys. Rev. Lett.*, 2006, **96**, 216104.
38 Y. Ding, Y. Zhou, J. Yao, C. Szymanski, J. Fredrickson, L. Shi, B. Cao, Z. Zhu and X.-Y. Yu, *Anal. Chem.*, 2016, **88**, 11244–11252.
39 W. Li, H. Li, J. Li, X. Cheng, Z. Zhang, F. Chai, H. Zhang, T. Yang, P. Duan, D. Lu and Y. Chen, *J. Environ. Sci.*, 2018, **69**, 61–76.
40 J. Wei, A. Bristow, E. McBride, D. Kilgour and P. B. O'Connor, *Anal. Chem.*, 2014, **86**, 1567–1574.
41 NIH, PubChem, https://pubchem.ncbi.nlm.nih.gov/, accessed April 15, 2019.

42 V. Khare, W. A. Sakarchi, P. N. Gupta, A. D. M. Curtis and C. Hoskins, *RSC Adv.*, 2016, **6**, 60126–60137.
43 L. Y. Kong, B. G. Su, Z. B. Bao, H. B. Xing, Y. W. Yang and Q. L. Ren, *J. Chromatogr. A*, 2011, **1218**, 8664–8671.
44 J. Lu, Y. Huang, W. Zhao, Y. Chen, J. Li, X. Gao, R. Venkataramanan and S. Li, *Mol. Pharmaceutics*, 2013, **10**, 2880–2890.
45 K. Tanaka, *J. Chem. Soc., Faraday Trans.*, 1978, **74**, 1879–1881.
46 E. E. Perez, A. A. Carelli and G. H. Crapiste, *J. Food Eng.*, 2011, **105**, 180–185.
47 S. E. M. Hamam, *J. Environ. Sci. Health, Part A: Environ. Sci. Eng.*, 1987, **22**, 445–456.
48 J. Won, S. W. Baek, H. Kim and H. Lee, *Energies*, 2019, **12**, 1963.

C. A Brief Report on Liquid NMR Diffusion Analysis of Bilge

By Kee Sung Han, Pacific Northwest National Laboratory

Experimental Details

All NMR measurements were performed on a 500 MHz NMR spectrometer equipped with a 5-mm liquid NMR probe, which has z-gradient capability with a maximum gradient strength of ~50 G/cm. The ^{1}H pulsed field gradient (PFG) NMR measurements were performed with a 13-interval bipolar gradients stimulated echo sequence (Dbppste, a vender supplied pulse sequence, Agilent, USA) at 25 °C. Diffusion coefficients were calculated from the PFG echo profile obtained as a function of gradient strength (g) using a Stejskal-Tanner equation: $S(g) = S(0)\exp[-D(\gamma\delta g)^2(\Delta-\delta/3)]$, where S(g) and S(0) are the echo peak height at the gradient strength of 0 and g, respectively, γ is the gyromagnetic ratio of proton (^{1}H), δ is the duration of gradient pulse, g is the gradient amplitude and Δ is the duration between the two pair of bipolar gradient pulses.

Initial Results

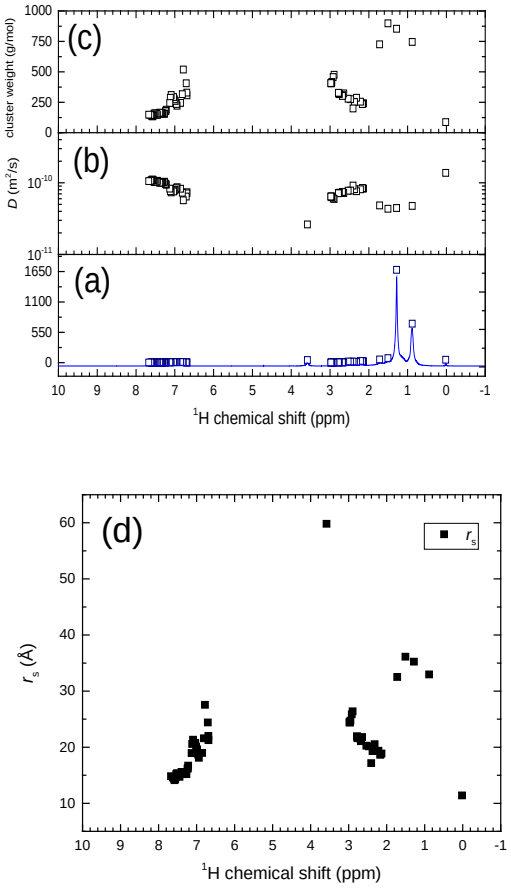

Figure A1 (a) ^{1}H NMR spectrum of fresh diesel with 10 µL tetramethylsilane (TMS, molecular weight ≈ 88.23 g/mol), (b) diffusion coefficients distribution of fresh diesel obtained from pulsed field gradient (PFG) NMR, (c) the cluster size (weight) calculated from the diffusion coefficients using the external calibration curve with TMS as a

reference molecule and (d) the hydrodynamic radius calculated from the diffusion coefficients using the Stokes-Einstein equation (D= $k_B T/6\pi\eta r_s$)

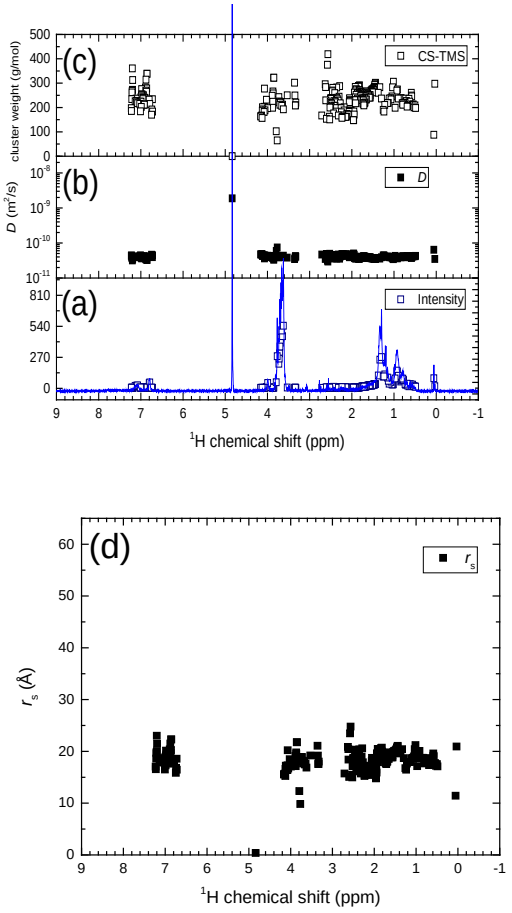

Figure A2 (a) ^{1}H NMR spectrum of fresh diesel diluted with D_2O (10:1) and 10 µL tetramethylsilane (TMS, molecular weight ≈ 88.23 g/mol) was added as an internal reference for cluster size calibration, (b) diffusion coefficients distribution of diluted diesel obtained from pulsed field gradient (PFG) NMR, (c) the cluster size (weight) calculated from the diffusion coefficients using the external calibration curve with TMS as a reference molecule and (d) the hydrodynamic radius calculated from the diffusion coefficients using the Stokes-Einstein equation (D= $k_B T/6\pi\eta r_s$).

^{1}H NMR spectrum shown in Figure 1(a) is the first echo signal on PFG-echo profile for fresh diesel sample and the open squares are the peak intensities used for the calculation of diffusion coefficients (shown in Figure 1(b)). The cluster weight (g/mol) were estimated using external calibration curve [1] with tetramethylsilane (TMS) reference. It showed the cluster sizes distributed in the region of 140 – 900 g/mol. In Figure 1(d) the distribution of hydrodynamic radius were estimated using the Stokes-Einstein equation: D= $k_B T/6\pi\eta r_s$, where, k_B is the Boltzmann constant, T absolute temperature, η is the viscosity and r_s is the hydrodynamic radius of diffusing molecules.

$D_{TMS}/D_x = r_{sx}/r_{sTMS}$ then $r_{sx} = r_{sTMS}$ (D_{TMS}/ D_x), where $r_{s,TMS}$ is 11.4 Å [2]

For fresh diesel sample, the hydrodynamic radius are distributed from 14 -36 Å.

For the diluted diesel (10: 1 vol. D_2O: diesel) solution, Figure 2 shows the first spectrum of ^1H PFG-echo profile and peak intensities used for diffusion calculation (Figure 2(a)), distributions of diffusion coefficient (Figure 2(b)), cluster weight (Figure 2(c)) and hydrodynamic radius (Figure 2(d)). While the peak intensities around 4 ppm were very tiny in diesel sample, the peak intensities on the chemical shift around 4 ppm is predominant in the diluted diesel solution. The cluster sizes were slightly reduced from those of pristine diesel and distributed around 100 – 400 g/mol. The hydrodynamic radius also reduced slightly and distributed around 15 – 25 Å

References

1. Neufeld, R. and D. Stalke, Accurate molecular weight determination of small molecules via DOSY-NMR by using external calibration curves with normalized diffusion coefficients. Chemical Science, 2015. **6**(6): p. 3354-3364.

2. Šoltésová, M., et al., Determination of Size of Molecular Clusters of Ethanol by Means of NMR Diffusometry and Hydrodynamic Calculations. The Journal of Physical Chemistry B, 2014. **118**(24): p. 6864-6874.